



Synthesis, characterization and catalase-like activity of the tetranuclear iron(III) complex involving a $(\mu\text{-oxo})(\mu\text{-hydroxo})\text{bis}(\mu\text{-alkoxo})\text{tetra}(\mu\text{-carboxylato})\text{tetrairon}$ core



Bianca M. Pires^a, Daniel M. Silva^a, Lorenzo C. Visentin^{a,1}, Valderes Drago^b, Nakédia M.F. Carvalho^{a,*}, Roberto B. Faria^a, O.A.C. Antunes^{a,2}

^a Universidade Federal do Rio de Janeiro, Instituto de Química, Avenida Athos da Silveira Ramos, 149 CT, Bloco A – 6º andar, Cidade Universitária, Rio de Janeiro 21945-970, RJ, Brazil

^b Universidade Federal de Santa Catarina, Departamento de Física, Trindade, Florianópolis 88040-900, SC, Brazil

ARTICLE INFO

Article history:

Received 2 December 2012

Received in revised form 15 July 2013

Accepted 15 July 2013

Available online 27 July 2013

Keywords:

Catalase-like activity

Michaelis–Menten kinetics

Tetranuclear iron(III) complex

ABSTRACT

The synthesis, characterization and catalase-like activity of the tetranuclear complex $[\text{Fe}_4(\mu\text{-O})(\mu\text{-OH})(\mu\text{-OAc})_4(\text{L})_2](\text{ClO}_4)_3$ (HL is the ligand 1,3-bis[(2-aminoethyl)amino]-2-propanol) is described herein. The complex was obtained from the self-assembly of $\text{Fe}(\text{ClO}_4)_3 \cdot x\text{H}_2\text{O}$, $\text{NaOAc} \cdot 3\text{H}_2\text{O}$ and HL. The X-ray structural elucidation, together with spectroscopic and ESI-MS data, disclosed a $(\mu\text{-oxo})(\mu\text{-hydroxo})\text{-bis}(\mu\text{-alkoxo})\text{tetra}(\mu\text{-carboxylato})\text{tetrairon}$ core structure that can be described as a dimer of dimer, where the four metallic centers are embedded in the same chemical environment. The kinetics of the catalase-like activity was investigated in water, TRIS buffer and acetonitrile, and it revealed a Michaelis–Menten behavior. The progress of H_2O_2 disproportionation reactions was followed by UV–Vis, ESI-MS/Q-TOF and EPR, indicating the disruption of the tetranuclear core, which was accelerated at higher proton concentration. The rate constant was higher in CH_3CN than in aqueous solution ($k_{\text{obs}}(\text{CH}_3\text{CN}) > k_{\text{obs}}(\text{buffer}) > k_{\text{obs}}(\text{H}_2\text{O})$).

© 2013 Elsevier B.V. All rights reserved.

1. Introduction

Although hydrogen peroxide is not a toxic compound, it generates the hydroxyl radical that causes lipid peroxidation, membrane damage and cell death [1]. The biological defense against hydrogen peroxide is accomplished by the catalase enzyme that converts it into water and dioxygen Eq. (1) [2–4].



Two main classes of catalase enzymes are known, an iron- and a manganese-based proteins. Although these catalases have different structural features, they perform the same biological activity. The first class is a heme-type catalase containing an iron(III)-protoporphyrin IX prosthetic group in the active site [5–7] and the second one is a binuclear manganese enzyme (MnCAT) [8–9]. In the later, a histidine and a glutamate residue are coordinated to each

manganese atom. Three bridges link the metal ions, a glutamate, and two bridges that have not been reliably established yet, which could be oxo, hydroxo or aquo.

In stress conditions, the organism can fail in protecting itself against radicals and the natural defenses might be insufficient [1]. Since the natural enzyme is unstable in solution and cannot be used as drug, synthetic models that reproduce its structural features and/or activity have potential biomedical application as therapeutic agents against oxidative stress [10–12]. Most of the synthetic models for MnCAT are manganese complexes, including mono [13–15] and dinuclear [16–20] compounds in the great majority and a few examples of trinuclear and tetranuclear as well [21–23]. Although the iron catalase enzyme is a heme-type, several non-heme dinuclear [24–29] and mononuclear [12,29,30] iron complexes were also able to promote hydrogen peroxide dismutation. However, no tetranuclear iron complex was described as a catalase model.

Tetranuclear oxo-, hydroxo- or alkoxo-bridged iron complexes are of interest from a bioinorganic viewpoint, since similar bridged moieties are present in the active site of numerous proteins. The main types of tetranuclear iron complexes are listed below and the structures are represented in Chart 1.

- “butterfly”: possesses the core $[\text{Fe}_4(\mu_3\text{-O})_2]^{8+}$ or $[\text{Fe}_4(\mu_3\text{-OR})_2]^{10+}$ (R = H, Me) [31–33];

* Corresponding author. Address: Universidade do Estado do Rio de Janeiro, Instituto de Química, Rua São Francisco Xavier, 524 Edifício Haroldo Lisboa da Cunha, IQ, Sala 407, Maracanã, 20550-013 Rio de Janeiro, RJ, Brazil. Tel.: +55 21 23340563; fax: +55 21 23340159.

E-mail address: nakedia@uerj.br (N.M.F. Carvalho).

¹ Present address: R&D NanoBusiness, e-Diffraction Pharma, CEP: 22451-900 Rio de Janeiro, RJ, Brazil.

² In memoriam.

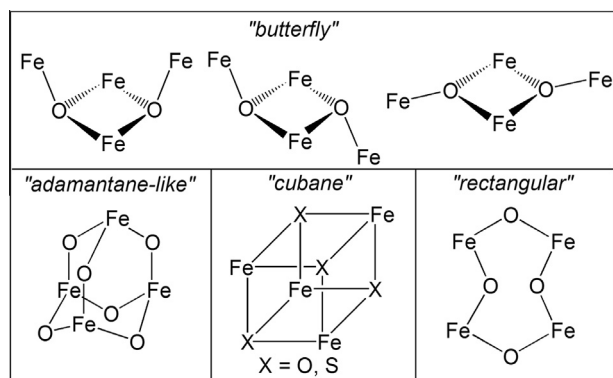


Chart 1. Main types of tetranuclear iron cores.

- adamantane-like: possesses the core $[\text{Fe}_4(\mu\text{-X})_2(\mu\text{-OH})_2(\mu\text{-O})_2]^{4+}$ (X = hydroxo, alkoxo or phenoxo) [34–36];
- cubane: consists of a $[\text{Fe}_4(\text{OR})_6]^{6+}$ core, with the iron atoms located at the corners of a cubane [33];
- rectangular: presents two separated cores, consisting of $\text{Fe}_2(\mu\text{-X})(\mu\text{-carboxilato})_n$, where X can be O, OH or alkoxo and $n = 0, 1, 2$. The two cores are linked by two oxo, two alkoxo bridges or two hydrocarbon chains [37–44].

In this work, we have synthesized the tetranuclear non-heme complex $[\text{Fe}_4(\mu\text{-O})(\mu\text{-OH})(\mu\text{-OAc})_4(\text{L})_2](\text{ClO}_4)_3$, where HL is the ligand 1,3-bis[(2-aminoethyl)amino]-2-propanol, and we have studied its catalase-like activity in water, TRIS buffer and acetonitrile, as well as its kinetics, in order to disclose if tetranuclear iron(III) complexes would be able to promote hydrogen peroxide dismutation, and what similarities they would share with the MnCAT enzyme. The monitoring of the H_2O_2 disproportionation reactions was carried out by UV–Vis, ESI-MS/Q-TOF and EPR.

2. Experimental

2.1. Materials and measurements

The reagents and solvents were used as received from commercial sources. The ligand 1,3-bis[(2-aminoethyl)amino]-2-propanol was synthesized from epichlorohydrin and ethylenediamine, as described in literature [45].

Solution UV–Vis spectra were recorded on a Shimadzu 1601PC spectrophotometer in water, TRIS buffer and CH_3CN , and diffuse reflectance UV–Vis spectra were recorded on a Shimadzu UV-2450 spectrophotometer. Infrared spectra were collected on a FTIR Nicolet Magna-IR 760 spectrophotometer (KBr or CsI pellets or as film in NaCl window). ^1H NMR and ^{13}C NMR spectra were obtained with a Bruker DRX-200 spectrometer in D_2O and the chemical shifts were referenced to the solvent peak.

Mössbauer spectra were obtained using a Wissel instrument in the constant acceleration mode with transmission geometry where the 20 mCi $^{57}\text{Co}/\text{Rh}$ source was maintained at room temperature. The resultant spectra were least square fitted to Lorentzian-shaped lines using the NORMOS software (Wissel Company). Metallic iron was used for energy calibration and also as reference for the isomer shift (δ) scale.

Electron paramagnetic resonance (EPR) measurements of the powder and solution materials were conducted on an EPR BRUKER EMX microX spectrometer (frequency X, band 9.5 GHz) at room temperature and 77 K (using liquid N_2), using the perpendicular microwave polarization (perpendicular polarization CW-EPR).

ESI-MS spectra of the complex in an acetonitrile solution in presence of H_2O_2 were acquired by using a quadrupole/time-of-flight (Q-ToF) mass spectrometer (Micromass, Manchester,

UK). General conditions were as follows: source temperature of 100 °C, capillary voltage of 3.5 kV, and cone voltage of 15–50 V. Mass spectra were acquired by scanning over the 90–1500 m/z range. The product ion MS analysis was accomplished with the orthogonal TOF (time-of-flight) analyzer.

Cyclic voltammetry experiments were carried out in acetonitrile and water using a BAS Epsilon potentiostat/galvanostat and a three-electrode system, consisting of a glassy carbon disk as the working electrode, a platinum wire as the auxiliary electrode and an Ag/AgCl system as the reference electrode. A 0.1 mol dm^{-3} solution of tetrabutylammonium hexafluorophosphate or of lithium perchlorate was used as supporting electrolyte for the analyses in acetonitrile or water, respectively. The Fc/Fc^+ ($E_{1/2} = 0.249$ V versus Ag/AgCl; $\Delta E = 125$ mV) or $\text{K}_3[\text{Fe}(\text{CN})_6]$ ($E_{1/2} = 0.254$ V versus Ag/AgCl; $\Delta E = 347$ mV) was used as internal standard for the analyses in acetonitrile or water, respectively. Spectroscopic grade solvent was used and the solutions were purged thoroughly with argon and kept under a positive pressure of this gas during the experiments. Potentials are expressed versus Fc/Fc^+ (0.400 V versus ENH) [46] for both scans at 25 and 100 mV/s in acetonitrile solutions and versus NHE ($E_{1/2}[\text{K}_3[\text{Fe}(\text{CN})_6]] = 0.361$ V vs ENH) at 100 mV/s in aqueous solutions [47].

Gas chromatography analyses were conducted on a HP5890 gas chromatograph with a HPDB5 column (30 m \times 0.25 mm \times 0.25 μm) connected to a FID detector, using H_2 (140 kPa) as carrier gas. The analysis conditions for the cyclohexane oxidation reactions were: initial temperature of 50 °C, heating ramp of 1.5 °C/min to 56 °C, then heating ramp of 10 °C/min to the final temperature of 127 °C. The injector and detector temperature was 200 °C and 250 °C, respectively. Products were identified by their mass spectra and the retention times were compared with those of authentic samples. Quantification was made through calibration plots for the detector response of the authentic samples.

Caution! The perchlorate salts used in this study are potentially explosive and should be handled with care!

2.2. Synthesis of the complex $[\text{Fe}_4(\mu\text{-O})(\mu\text{-OH})(\mu\text{-OAc})_4(\text{L})_2](\text{ClO}_4)_3$

The complex $[\text{Fe}_4(\mu\text{-O})(\mu\text{-OH})(\mu\text{-OAc})_4(\text{L})_2](\text{ClO}_4)_3$ was synthesized by addition of the ligand solution (3.7 mmol, 0.65 g in 10.0 cm^3 of ethanol) to a solution of $\text{Fe}(\text{ClO}_4)_3 \cdot x\text{H}_2\text{O}$ (4.4 mmol, 1.56 g) and $\text{NaOAc} \cdot 3\text{H}_2\text{O}$ (4.4 mmol, 0.60 g) in 30.0 cm^3 of ethanol. A green precipitate was immediately formed, which was filtered and washed with ethanol. The solid was recrystallized in acetonitrile. After few days, green single crystals suitable for X-ray analysis were obtained. Yield: 0.68 g.

Anal. Calc. for $\text{C}_{22}\text{H}_{51}\text{N}_8\text{O}_{24}\text{Cl}_3\text{Fe}_4 \cdot 1.5\text{C}_2\text{H}_5\text{OH}$: C, 24.80; H, 5.00; N, 9.26. Found: C, 24.96; H, 4.72; N, 9.19%. FTIR (CsI, cm^{-1}): 3466, 3343, 3275, 3223, 3125, 2938, 2892, 1584, 1457, 1427, 1101, 986, 654, 625. UV–Vis in CH_3CN ; λ/nm ($\epsilon/\text{dm}^3 \text{mol}^{-1} \text{cm}^{-1}$): 635 (6.88×10^1), 475 (5.03×10^2), 316 (1.07×10^4), 217 (2.81×10^4), 242 (2.00×10^4).

2.3. Crystal structure of $[\text{Fe}_4(\mu\text{-O})(\mu\text{-OH})(\mu\text{-OAc})_4(\text{L})_2](\text{ClO}_4)_3$

The X-ray data were collected at 295 K from an Enraf–Nonius Kappa-CCD [48] diffractometer with graphite monochromatized $\text{Mo K}\alpha$ radiation. The cell parameters were obtained using COLLECT [48] and PHICHI [49] softwares, and were refined using DIRAX [50] software. Intensities were corrected by Lorentz polarization with EvalCCD [51] program and absorption with SADABS [52] software. The structure was solved by SHELXS-97 Direct Methods [53], and refined with SHELXL-97 [54]. The positional parameters of the H atoms bonded to C atoms in the methylene groups were obtained geometrically, with the C–H distances fixed at 0.96 Å for Csp^3 atoms, and set to ride on their respective C atoms, with $U_{\text{iso}}(\text{H}) = -1.2U_{\text{eq}}$

(Csp³). The hydrogen from methyl groups were obtained geometrically and ideally disordered in the two positions, with the C–H distances fixed at 0.97 Å for Csp³ atoms and $U_{\text{iso}}(\text{H}) = -1.5U_{\text{eq}}(\text{Csp}^3)$ for respective C atoms. The positional parameters of H3o atom in the O2···H3o–O3 moiety were obtained from difference Fourier map and refined with an isotropic displacement parameter.

The squeeze [55] procedure was adopted because disorder effect was observed in 3 water molecules that act as solvate of crystallization. Before the squeeze procedure, these water molecules occupied 488.6 Å³ in the unit cell; after the squeeze, this space is void after the exclusion of 54 electrons per unit cell. X-ray data are collated in Table 1.

2.4. Catalase-like activity

2.4.1. H₂O₂ disproportionation reactions

The catalase-like activity was followed by measuring the volume of O₂ produced. The total reaction volume was kept constant during all experiments at 5.0 mL. The reactions were performed at 25 °C, using the assistance of a water bath and a thermostat. Water, TRIS buffer or CH₃CN was used as solvent. The buffer pH was adjusted to 7.2 with HCl. The reactor was a kitassato flask (25 cm³) magnetically stirred and closed with a rubber septum. The kitassato was connected to an inverted graduated burette filled with water. Hydrogen peroxide solution (commercial 30% aqueous solution) was injected through the septum with a syringe and the dioxygen production was measured in the burette at appropriate times. The experimental data were plotted in a curve describing the amount of dioxygen evolved versus time. Observed initial rates were expressed as mol(O₂) s⁻¹ and calculated from the maximum slope of the curves describing the O₂ evolution versus time.

The pH variation during the reaction in water was evaluated for 30 min, using a pHmeter. The reaction was carried out in a glass

Table 1
Crystal data and structure refinement for [Fe₄(μ-O)(μ-OH)(μ-OAc)₄(L)₂](ClO₄)₃.

Empirical formula	C ₂₂ H ₅₁ N ₈ O ₂₄ Cl ₃ Fe ₄ ·3H ₂ O
Formula weight	1141.46, 1195.52
T (K)	295(2)
Wavelength (Å)	0.71073
Crystal system	Orthorhombic
Space group	Pmnn
Unit cell dimensions	
a (Å)	17.177(3)
b (Å)	15.637(3)
c (Å)	17.229(3)
V (Å ³)	4627.7(14)
Z	4
D _{calc} (Mg/m ³)	1.638
Absorption coefficient (mm ⁻¹)	1.488
F(000)	2344
Crystal size (mm)	0.15 × 0.11 × 0.08
θ (°)	2.37–24.50
Index ranges	−17 ≤ h ≤ 18, −18 ≤ k ≤ 18, −19 ≤ l ≤ 20
Reflections collected	34,095
Independent reflections (R _{int})	3897 (0.0413)
Completeness to theta = 24.5° (%)	97.4
Absorption correction	semi-empirical from equivalents
Maximum and minimum transmission	0.8902 and 0.8076
Refinement method	Full-matrix least-squares on F ²
Data/restraints/parameters	3897/0/315
Goodness-of-fit (GOF) on F ²	1.088
Final R indices [I > 2σ(I)]	R ₁ = 0.0581, wR ₂ = 0.1713
R indices (all data)	R ₁ = 0.0786, wR ₂ = 0.1868
Largest difference in peak and hole (e Å ⁻³)	1.190 and −0.901

tube under stirring, with the complex concentration of 2.5 × 10⁻³ M and the H₂O₂ concentration of 0.5 M.

2.4.2. Influence of the TRIS buffer in the H₂O₂ disproportionation reactions

Three different buffer solutions were prepared at pH 7.2, with TRIS concentrations of 0.1, 0.25 and 0.5 M. A typical H₂O₂ disproportionation experiment was conducted using the buffer solutions to prepare the complex solutions, with the final concentration of 1.25 × 10⁻³ M. 0.11 mL of an aqueous 30% solution of H₂O₂ was added, at a final concentration of 0.25 M. The O₂ volume evolved was measured with a burette. The total reaction volume was of 5.0 mL.

2.4.3. Kinetics of the H₂O₂ disproportionation reactions

In a typical disproportionation experiment the concentration of the reagents was varied to determine the dependence of the initial rate on the dioxygen evolution. In a first set of experiments, the hydrogen peroxide concentration was kept constant while the concentration of the complex was varied. In a second set of experiments, the opposite was done: the hydrogen peroxide concentration was varied while the complex concentration was kept constant. The concentration values for each solvent are listed in Table 2.

2.4.4. Progress of H₂O₂ disproportionation reactions followed by UV-Vis, ESI-MS/Q-TOF and EPR

The UV-Vis experiments were conducted in water, 0.25 M of TRIS buffer at pH 7.2 or in CH₃CN. 30 μL of 30% aqueous solution of H₂O₂ ([H₂O₂]₀ = 0.1 M) were added to 3.0 mL of the complex solution at 1.5 × 10⁻³ M in the respective solvent and the electronic spectra were acquired in every two minutes during one hour.

The ESI-MS experiments were conducted in CH₃CN. 50 μL of 30% aqueous solution of H₂O₂ ([H₂O₂]₀ around 0.1 M) were added to 1.0 mL of the complex solution around 1 × 10⁻⁵ M. Mass spectra were acquired in the region of m/z 90–1300, before and soon after de addition of H₂O₂, and after 3, 6 and 20 min of reaction. In the experiments in pure water, no ionized species were detected.

The EPR experiments were conducted in CH₃CN at 77 K. 100 μL of 30% aqueous solution of H₂O₂ ([H₂O₂]₀ = 0.1 M) were added to 10 mL of the complex solution at 1.0 × 10⁻⁵ M. Aliquots of the reaction were taken at the appropriate time (0, 3, 6, 9 and 20 min), frozen at 77 K and analyzed.

2.5. Cyclohexane oxidation

Cyclohexane oxidation tests were carried out in water and CH₃CN, using H₂O₂ as oxidant. The catalyst:substrate:oxidant ratio was of 1:1000:1000 with the catalyst concentration of 7 × 10⁻⁴

Table 2
Complex and H₂O₂ concentration for the kinetics experiments.

Experiment		Solvent		
		Water	TRIS buffer	CH ₃ CN ^a
Complex effect	[H ₂ O ₂] ₀ /M	5.00 × 10 ⁻¹	5.00 × 10 ⁻¹	1.00 × 10 ⁻¹
	[complex] ₀ /M	4.58 × 10 ⁻⁴	5.00 × 10 ⁻⁴	1.00 × 10 ⁻⁴
H ₂ O ₂ effect	[H ₂ O ₂] ₀ /M	2.29 × 10 ⁻³	2.50 × 10 ⁻³	5.00 × 10 ⁻⁴
	[complex] ₀ /M	0.24–3.00	0.13–1.00	0.075–0.195
		1.14 × 10 ⁻³	1.25 × 10 ⁻³	7.5 × 10 ⁻⁵

^a The volume of CH₃CN was kept constant in all experiments at 4.6 mL. The initial H₂O₂ solution was diluted with H₂O, in order to keep the water volume constant at 0.4 mL for all experiments.

mol dm⁻³. The reaction was quenched by addition of an aqueous 0.4 M Na₂SO₄ solution, followed by extraction with 10 mL of diethyl ether. The ether layer was dried with anhydrous Na₂SO₄ and analyzed by GC-FID. The reaction samples were analyzed before and after reaction with PPh₃ to determine the corrected yield of the products, accounting for the decomposition of cyclohexyl hydroperoxide in the chromatograph [56]. Adipic acid was quantified by titration experiments with NaOH.

3. Results and discussion

3.1. Synthesis

The ligand was synthesized from epichlorohydrin and ethylenediamine, according to a published procedure [45]. The green complex [Fe₄(μ-O)(μ-OH)(μ-OAc)₄(L)₂](ClO₄)₃ was prepared by the self-assembly of HL, Fe(ClO₄)₃·xH₂O and NaOAc·3H₂O, as shown in Scheme 1. The title complex presents the rectangular tetranuclear iron(III) core mentioned above. Several of the rectangular complexes reported have been obtained from ligands containing the 1,3-diamino-2-propanol backbone [57–59], although binuclear complexes have also been described with such ligands [60,61]. It seems that the carboxylate bridge (R-CO₂⁻) plays an important role in the nuclearity of the complex. In general, when small R groups are used, such as acetate, tetranuclear complexes are obtained and with larger R groups, such as benzoate, binuclear complexes are formed.

3.2. X-ray crystallographic study

Single crystal X-ray analysis of [Fe₄(μ-O)(μ-OH)(μ-OAc)₄(L)₂](ClO₄)₃, in accordance with spectroscopic and ESI-MS analyses, disclosed the rectangular tetranuclear iron(III) complex. The atom arrangement and numbering schemes of the complex cation are shown in Fig. 1.

The complex can be described as a dimer of dimers, where the N,O-pentadentate ligand links two iron atoms through the alkoxo bridge. Four carboxylate, one oxo and one hydroxo bridges connect a pair of dimers, leading to a (μ-oxo)(μ-hydroxo)bis(μ-alkoxo)tetra(μ-carboxylato)tetrairon core. Each iron atom has a N₂O₄ donor set in a distorted octahedron geometry. The four iron atoms are equivalent, consistent with the Mössbauer spectra (see below), and lay in the corners of a rectangle, that could be considered as a square judging by the almost identical side lengths (Fig. 2A). A plane is formed with the iron atoms, the alkoxo bridges and with two of the carboxylato bridges (Fig. 2). The two remaining acetate bridges are pointing upwards and the oxo and hydroxo bridges are downwards, as is better seen in Fig. 2B and C. On the other hand, the carboxylato, oxo and hydroxo bridges are located on special

sites, some of whose atoms are located on one mirror plane. The m symmetry includes the following atoms: O3, H3o, O2, C8–C9, C10–C11, C12–C13, and C14–C15. The symmetry code used to generate the other half of the molecule is (-x, y, z), with the perpendicular mirror plane [100].

The ligand nitrogen atoms from the primary [Fe1–N1 2.058(6) Å; Fe2–N4 2.145(5) Å] and secondary amines [Fe1–N2 2.341(5) Å; Fe2–N3 2.318(5) Å] as well as the oxygen from the alkoxo are in a facial arrangement. The alkoxo group forms with the coordinated iron atoms an angle of 122.79(18)° Fe1–O1–Fe2 [Fe1–O1 1.983(3) Å; Fe2–O1 2.007(3) Å]. The bridging oxygen atoms from the oxo and hydroxo groups are bound slightly asymmetrically to two different iron centers [Fe2–O2 1.972(2) Å and Fe1–O3 2.008(2) Å], which show bond angles of 123.3(2)° along Fe1–O3–Fe1ⁱ and 127.3(2)° along Fe2–O2–Fe2ⁱ [Symmetry code (i) = -x, y, z].

A distorted geometry around Fe1 and Fe2 is a consequence of the different types of bridges and of the different basic character of the N-donor ligand atoms. The mean bond angles around Fe1 in the equatorial arrangement are 166.97(16)° O7–Fe1–O1 and

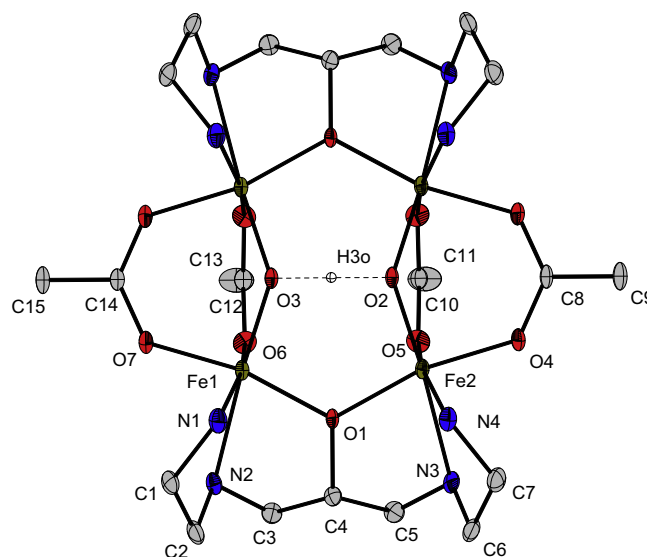
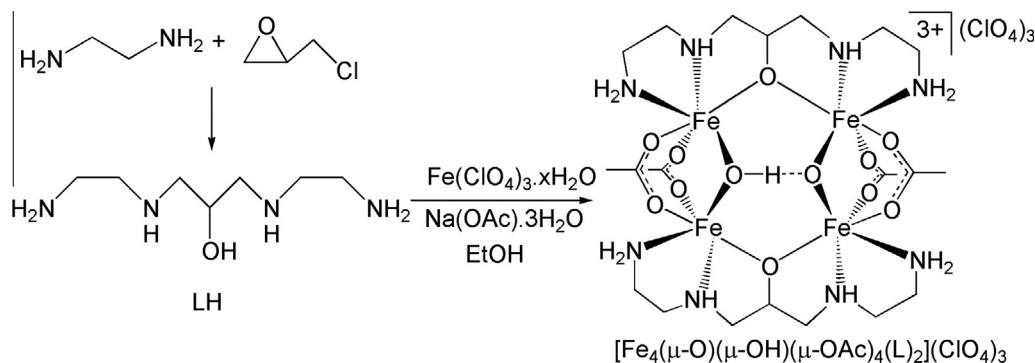


Fig. 1. ORTEP plot of the cation of [Fe₄(μ-O)(μ-OH)(μ-OAc)₄(L)₂](ClO₄)₃. View of the arrangements, numbering scheme and intramolecular H-bond, with thermal ellipsoids at the 20% probability level. Hydrogen atoms have been omitted. Bond lengths (Å): 1.536(9) N1–C1, 1.497(9) C1–C2, 1.456(7) C2–N2, 1.391(7) N2–C3, 1.511(7) C3–C4, 1.548(6) O1–C4, 1.396(7) C4–C5, 1.484(7) C5–N3, 1.506(8) N3–C6, 1.569(10) C6–C7 and 1.506(8) C7–N4; and angles: 131.2(6)° O7–C14–O7ⁱ, 131.9(6)° O6–C12–O6ⁱ, 131.4(6)° O5–C10–O5ⁱ and 131.1(6)° O4–C8–O4ⁱ. [Symmetry code (i) = -x, y, z].



Scheme 1. Synthesis of the complex [Fe₄(μ-O)(μ-OH)(μ-OAc)₄(L)₂](ClO₄)₃.

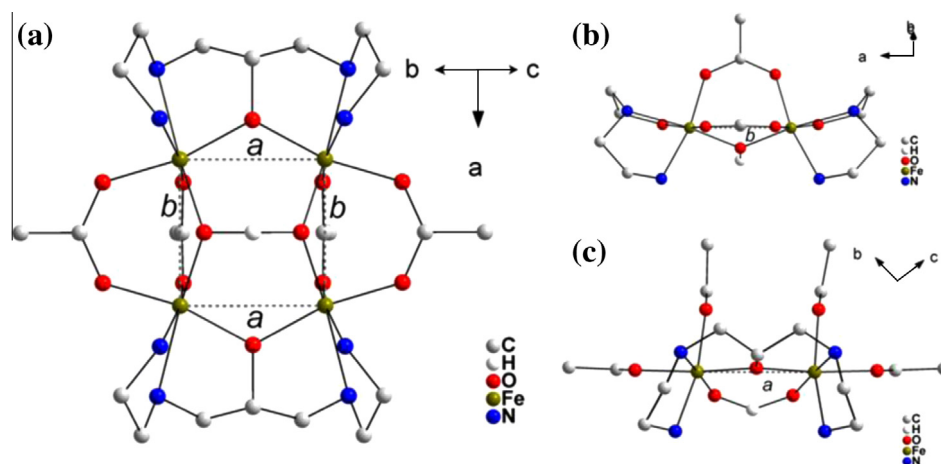


Fig. 2. Views of $[\text{Fe}_4(\mu\text{-O})(\mu\text{-OH})(\mu\text{-OAc})_4(\text{L})_2](\text{ClO}_4)_3$. $a = 3.503 \text{ \AA}$; $b = 3.534 \text{ \AA}$.

$172.79(15)^\circ$ O3–Fe1–N2, and in the axial position is $162.5(2)^\circ$ O6–Fe1–N1. For Fe2 in the equatorial arrangement the angles are $167.32(16)^\circ$ O4–Fe2–O1 and $172.86(15)^\circ$ O2–Fe2–N3 and in the axial position is $163.91(19)^\circ$ O5–Fe2–N4. Other selected bond lengths and angles are listed in the caption for Fig. 1.

The Fe \cdots Fe distance for the (μ -alkoxo)diiron moiety is $3.503(1) \text{ \AA}$ (a) and that for the (μ -oxo/ μ -hydroxo)bis(μ -carboxylato)diiron moiety are $3.535(1) \text{ \AA}$ and $3.534(1) \text{ \AA}$ (b). The a and b sides are pretty similar, and are defined in Fig. 2. The geometric parameters for these chemical bonds are in agreement with the data for similar structures [62,63]. Crystal structure of $\text{Na}[\text{Fe}_4(\text{dhpta})_2(\mu\text{-O})(\mu\text{-OH})(\mu\text{-Ala})_2]\cdot 6\text{H}_2\text{O}$, published by Tanase et al. [64], showed an average Fe \cdots Fe distance of 3.692 and 3.463 \AA (equivalent to a and b, respectively).

The O2 and O3 atoms deviate from their mean Fe1/Fe2/Fe2ⁱ/Fe1ⁱ equatorial plane by 0.2703 \AA . The dihedral angle between the equatorial arrangements O1/N2/O7/O3/Fe1 and O1/N3/O4/O2/Fe2 is $11.4(2)^\circ$. The mean torsion angles occurring on the ligand are $-43.5(5)^\circ$ in N4–C7–C6–N3, $-47.9(5)^\circ$ in N3–C5–C4–O1, $47.0(6)^\circ$ in O1–C4–C3–N2, and $48.5(7)^\circ$ in N1–C1–C2–N2.

An intramolecular classical hydrogen bond in a resonance system occurs between the atoms O2 and O3. The bond lengths in this O \cdots H–O moiety are $1.29(12)$ and $1.20(13) \text{ \AA}$ for O3–H3o and O2–H3o, respectively. The distance O2 \cdots O3 is $2.347(7) \text{ \AA}$ and the angle O2–H3o–O3 is $141(11)^\circ$, which are indicative of a strong hydrogen bond. $\text{Na}[\text{Fe}_4(\text{dhpta})_2(\mu\text{-O})(\mu\text{-OH})(\mu\text{-L-Ala})_2]\cdot 6\text{H}_2\text{O}$ [61] has a similar O–H \cdots O hydrogen bond, O1–H1o 1.22 \AA , O(2)–H1o 1.21 \AA , O1 \cdots O2 $2.426(4) \text{ \AA}$ and O1–H1o–O2 176.08° .

3.3. Infrared, electronic, Mössbauer and EPR spectroscopy

The FT-IR spectrum of the complex is characterized by absorptions at 1584 cm^{-1} (ν_{as}) and 1427 cm^{-1} (ν_{s}), which are assigned to the asymmetric and symmetric C=O vibrations of the acetate ligands, respectively. The difference $\Delta [\Delta = \nu_{\text{as}}(\text{CO}_2) - \nu_{\text{s}}(\text{CO}_2) = 157 \text{ cm}^{-1}]$ between the bands is characteristic of carboxylate group coordinated in a bidentate bridging mode [65]. Similar values were obtained for the complex $[\text{Fe}_4(\text{OHO})(\text{OH})_2(\text{O}_2\text{CMe})_4(\text{phen})_4](\text{ClO}_4)_3$, which possesses the same (μ -oxo)bis(μ -carboxylato)diiron(III) moiety [44]. The broad OH band around 3450 cm^{-1} in the ligand spectrum has disappeared after complexation, indicating the coordination of the alkoxo group to the iron. The perchlorate band was observed at 1101 cm^{-1} .

The UV–Vis spectra in CH_3CN are presented in Fig. 3(a). The band at 635 nm ($\epsilon = 6.88 \times 10^4 \text{ M}^{-1} \text{ cm}^{-1}$) and the shoulder at 410 nm can be attributed to the oxo-to-Fe^{III} (LMCT) transition. The band at 475 nm ($\epsilon = 5.03 \times 10^2 \text{ M}^{-1} \text{ cm}^{-1}$) is attributed to the ${}^6\text{A}_{1g} \rightarrow ({}^4\text{E}_g,$

${}^4\text{A}_{1g})$ ligand field transition. These data are in accordance with the electronic transitions reported for (μ -oxo)diiron(III) complexes [66–68]. Intense bands in the UV region was observed at 316 nm ($\epsilon = 1.07 \times 10^4 \text{ M}^{-1} \text{ cm}^{-1}$), 217 nm ($\epsilon = 2.81 \times 10^4 \text{ M}^{-1} \text{ cm}^{-1}$) and 242 nm ($\epsilon = 2.00 \times 10^4 \text{ M}^{-1} \text{ cm}^{-1}$). Comparison of the electronic spectra in solid state (diffuse reflectance) and in solution shows the same transitions around 635 and 475 nm , suggesting a similar structure in both cases. The spectra in water and buffer presented the same shapes of the spectra in CH_3CN , however the bands are less well defined, the bands at 306 and 488 nm appears as a shoulder. Furthermore, the band at 635 nm and the shoulder at 410 nm are not present, indicating that a possible loss of the oxo bridge may be occurring in aqueous solution.

The Mössbauer spectra of the complex recorded at 298 and 115 K are illustrated in Fig. 4. The room and low temperature spectra were least-squares fitted with Lorentzian lines and both consist of a single quadrupole doublet, which indicates a complete equivalence of the four iron centers. The isomer shift values ($\delta = 0.32 \text{ mm s}^{-1}/298 \text{ K}$; $\delta = 0.42 \text{ mm s}^{-1}/115 \text{ K}$) are typical of a high-spin Fe^{III} center. The quadrupole splitting values ($\Delta E_{\text{q}} = 1.02 \text{ mm s}^{-1}/298 \text{ K}$; $\Delta E_{\text{q}} = 1.01 \text{ mm s}^{-1}/115 \text{ K}$) do not vary with temperature, as expected, and the high values are indicative of low symmetry around the iron center due its asymmetric environment (N_2O_4). Considerably high values of ΔE_{q} were also observed for similar complexes which possess alkoxo bridges with 1,3-amino-2-propanol backbone and a NO_5 environment: $\text{Na}[\text{Fe}_4(\text{dhpta})_2(\mu\text{-O})(\mu\text{-OH})(\mu\text{-Ala})_2]$ ($\Delta E_{\text{q}} = 1.21 \text{ mm s}^{-1}/298 \text{ K}$) [64] and $(\text{Me}_2\text{NH}_2)_4[\text{Fe}_4(\text{dhpta})_2(\mu\text{-O})(\mu\text{-OH})(\mu\text{-O}_2\text{CCH}_3)_2](\text{NO}_3)$ ($\Delta E_{\text{q}} = 1.15 \text{ mm s}^{-1}/298 \text{ K}$) [62].

Solid-state EPR spectra (Fig. S6) of the title complex were collected at room temperature and at 77 K . The spectrum at room temperature was EPR silent and at 77 K two signals were observed at $g = 8$ and $g = 4.3$, both characteristics of a rhombic high-spin iron(III) center attributed to a mononuclear impurity present in the solid. The same EPR silent behavior was described for $[\text{Fe}_4(\text{OHO})(\text{OH})_2(\text{O}_2\text{CMe})_4(\text{phen})_4](\text{ClO}_4)_3$, which possesses the same (μ -oxo)bis(μ -carboxylato)diiron(III) moiety [44], indicating a strong antiferromagnetic coupling between the diiron(III) centers. The spectrum in CH_3CN (Fig. S7) was also EPR silent, what suggests that the tetranuclear structure of the complex is preserved in solution, as described for similar tetranuclear complexes in DMF as well [69].

3.4. Electrochemistry

The electrochemical behavior of the complex $[\text{Fe}_4(\mu\text{-O})(\mu\text{-OH})(\mu\text{-OAc})_4(\text{L})_2](\text{ClO}_4)_3$ was investigated by cyclic voltammetry. The redox processes in CH_3CN (Table 3) shows a strong

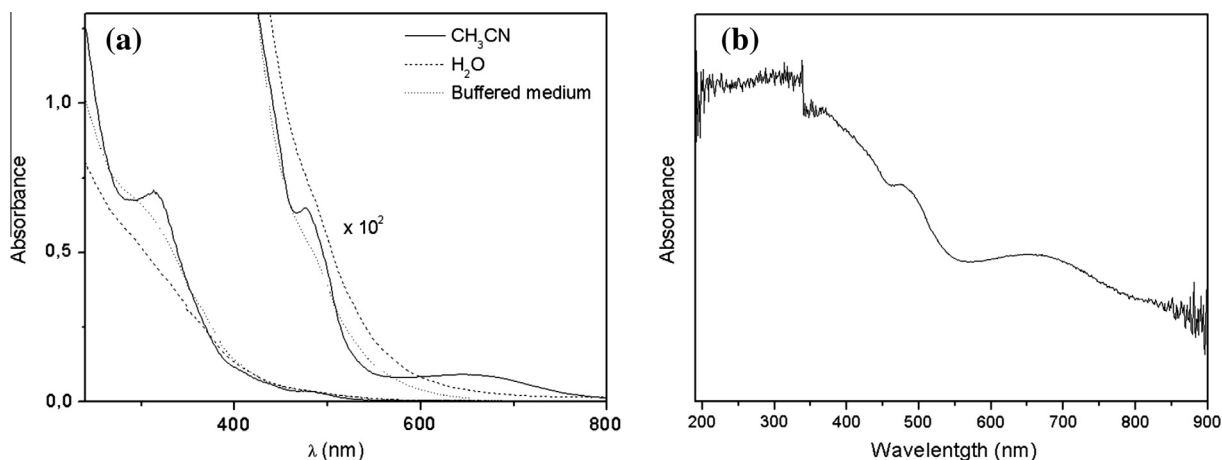


Fig. 3. Electronic spectra of $[\text{Fe}_4(\mu\text{-O})(\mu\text{-OH})(\mu\text{-OAc})_4(\text{L})_2](\text{ClO}_4)_3$: (a) solution and (b) diffuse reflectance-solid state.

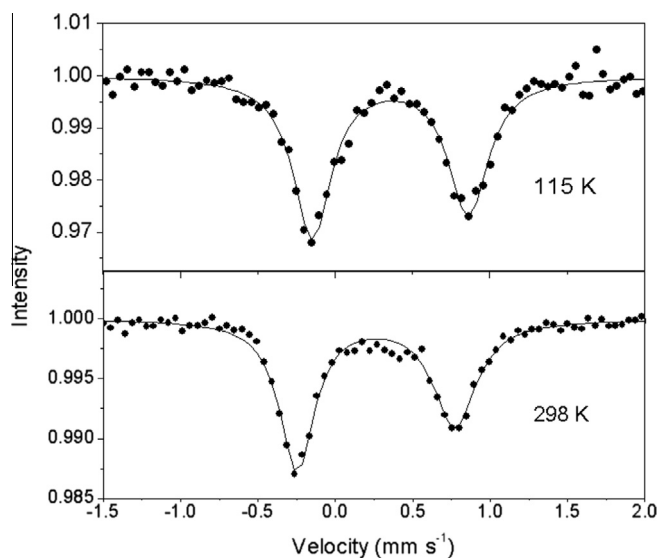


Fig. 4. ^{57}Fe Mössbauer spectra of $[\text{Fe}_4(\mu\text{-O})(\mu\text{-OH})(\mu\text{-OAc})_4(\text{L})_2](\text{ClO}_4)_3$, at 298 and 115 K.

dependence on the sweep rate. At 25 mV s^{-1} (Fig. 5(a)-inlet), two cathodic waves could be observed, the first (I) at $E_{\text{pc}}^{(I)} = -0.711 \text{ V}$ versus Fc/Fc^+ (-0.462 V versus Ag/AgCl) and the second (II) at $-E_{\text{pc}}^{(II)} = -1.093 \text{ V}$ versus Fc/Fc^+ (-0.844 V versus Ag/AgCl). The reduction waves could be observed at all sweep rates, while oxidation waves could be observed only at higher ones. It is possible that the reduced species formed at (I) and (II) have undergone some irreversible chemical reaction, being unavailable for a subsequent oxidative process. Although, at higher sweep rates, the newly formed species could be oxidized before its transformation [70]. As the sweep rate increases, a third reduction process (III) and three oxidation processes (IV, V, VI) appear. It is not possible to assure that these new oxidation processes are related to the reduction processes I, II and III, however, if they are related they do not correspond to reversible redox processes, even at 250 mV s^{-1} , due to the large ΔE values.

In order to compare our data with the literature at 100 mV s^{-1} , half-wave potential ($E_{1/2}^{(I/V)} = -0.580 \text{ V}$ versus Fc/Fc^+ ; -0.331 V versus Ag/AgCl) were calculated for (I) and (V). The $\Delta E^{(I/V)} = 153 \text{ mV}$, being characterized as a *quasi-reversible* process ($\Delta E = 125 \text{ mV}$ for Fc/Fc^+). Moreover, the cathodic and anodic waves

Table 3

Cyclic voltammetry data for $[\text{Fe}_4(\mu\text{-O})(\mu\text{-OH})(\mu\text{-OAc})_4(\text{L})_2](\text{ClO}_4)_3$.

	CH_3CN		H_2O
	25 mV s^{-1}	100 mV s^{-1}	100 mV s^{-1}
$E_{\text{pc}}(\text{V})$ vs. Ag/AgCl	$-0.462^{(I)}$; $-0.844^{(II)}$	$-0.407^{(I)}$; $-0.808^{(II)}$; $-1.019^{(III)}$	-0.408
$E_{\text{pa}}(\text{V})$ vs. Ag/AgCl	–	$-0.523^{(IV)}$; $-0.111^{(VI)}$	0.113
$E_{1/2}(\text{V})$ vs. Ag/AgCl	–	$-0.331^{(I/V)}$	-0.148
$E_{\text{pc}}(\text{V})$ vs. Fc/Fc^+	$-0.711^{(I)}$; $-1.093^{(II)}$	$-0.656^{(I)}$; $-1.057^{(II)}$; $-1.268^{(III)}$	–
$E_{\text{pa}}(\text{V})$ vs. Fc/Fc^+	–	$-0.772^{(IV)}$; $-0.36^{(VI)}$; $-0.503^{(V)}$	–
$E_{\text{pc}}(\text{V})$ vs. NHE	$-0.311^{(I)}$; $-0.693^{(II)}$	$-0.256^{(I)}$; $-0.657^{(II)}$; $-0.868^{(III)}$	-0.199
$E_{\text{pa}}(\text{V})$ vs. NHE	–	$-0.372^{(IV)}$; $0.04^{(VI)}$; $-0.103^{(V)}$	0.322
$\Delta E(\text{V})$	–	0.153	0.521
$\Delta E(\text{V})$ -internal standard	$0.125 (\text{Fc}^+/\text{Fc})$	$0.125 (\text{Fc}^+/\text{Fc})$	$0.347 (\text{K}_3[\text{Fe}(\text{CN})_6])$

do not have equal heights, and $i_{\text{pc}}^{(I/V)} > i_{\text{pa}}^{(I/V)}$ for all rates. The plot $i_{\text{pc}}^{(I/V)}$ versus $(v)^{1/2}$ is linear though, while the plot $i_{\text{pa}}^{(I/V)}$ versus $(v)^{1/2}$ is not, confirming the *quasi-reversible* behavior. The two reductions peaks at $E_{\text{pc}}^{(I)} = -1.057 \text{ V}$ versus Fc/Fc^+ and $E_{\text{pc}}^{(II)} = -1.268 \text{ V}$ versus Fc/Fc^+ could be observed at higher sweep rates, although, for smaller rates, a broad peak was observed instead. The oxidation peak (IV) at $E_{\text{pa}}^{(IV)} = -0.772 \text{ V}$ versus Fc/Fc^+ can be associated with one of these processes.

The tetranuclear complex $[\{\text{Fe}_2(\mu\text{-O})(\mu\text{-OAc})_2(\mu\text{-bpteta})_2\}]^{4+}$ (bpteta is 1,10-bis(2-pyridylmethyl)-1,4,7,10-tetraazadecane) exhibits a single irreversible cathodic wave at -0.62 V versus Ag/AgCl [41]. This value is close to the $E_{\text{pc}}^{(I)} = -0.656 \text{ V}$ versus Fc/Fc^+ (-0.407 V versus Ag/AgCl) for the title complex. The complex $[\text{LFe}_2\text{O}(\text{C}_5\text{H}_5\text{O}_4)]_2(\text{PF}_6)_4$ ($\text{L} = 1,4\text{-bis}(1,4,7\text{-triazol-1-cyclononyl})\text{butane}$) presents two reduction peaks at -0.500 and -0.635 V versus Ag/AgCl , respectively, which correspond, as seen in the reversed scan, to two oxidation peaks at -0.360 and -0.580 V . The complex $[(\text{L}3)_2\text{Fe}_2(\mu\text{-O})(\mu\text{-O}_2\text{CMe})_2](\text{ClO}_4)_2 \cdot 2\text{H}_2\text{O}$ ($\text{L}3 = N\text{-methyl-}N,N\text{-bis}(2\text{-pyridylmethyl})\text{amine}$) exhibits a *quasi-reversible* $\text{Fe}^{\text{III}}\text{Fe}^{\text{III}}/\text{Fe}^{\text{III}}\text{Fe}^{\text{II}}$ redox process at $E_{1/2} = -0.32 \text{ V}$ vs SCE and $\Delta E_p = 200 \text{ mV}$ [71]. Based on these complexes, process (I/V) can be assigned to the one-electron reduction process from $\text{Fe}^{\text{III}}\text{Fe}^{\text{III}}$ to $\text{Fe}^{\text{III}}\text{Fe}^{\text{II}}$ and the more anodic process (II or III/IV) to the reduction from $\text{Fe}^{\text{III}}\text{Fe}^{\text{II}}$ to $\text{Fe}^{\text{II}}\text{Fe}^{\text{II}}$.

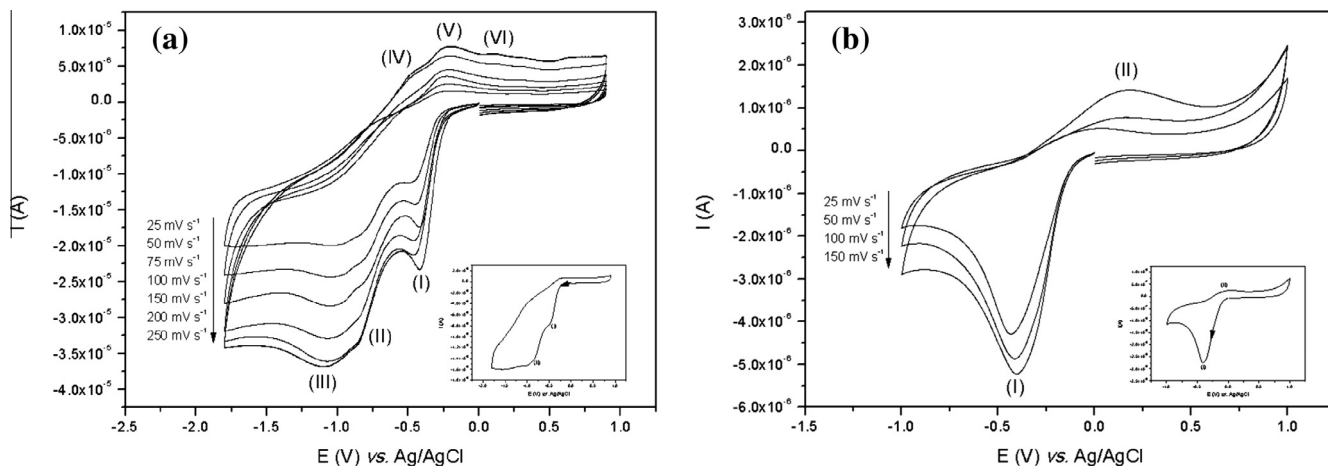


Fig. 5. Cyclic voltammogram of $[\text{Fe}_4(\mu\text{-O})(\mu\text{-OH})(\mu\text{-OAc})_4(\text{L})_2](\text{ClO}_4)_3$ at various sweep rates. (a) CH_3CN and (b) H_2O . Inlet: voltammogram at 25 mV s^{-1} . Ferrocene ($E_{1/2} = 0.239 \text{ V vs. Ag/AgCl}$; $\Delta E = 121 \text{ mV}$) or $\text{K}_3[\text{Fe}(\text{CN})_6]$ ($E_{1/2} = 0.254 \text{ V vs. Ag/AgCl}$; $\Delta E = 347 \text{ mV}$) was used as internal standard, in CH_3CN or H_2O , respectively.

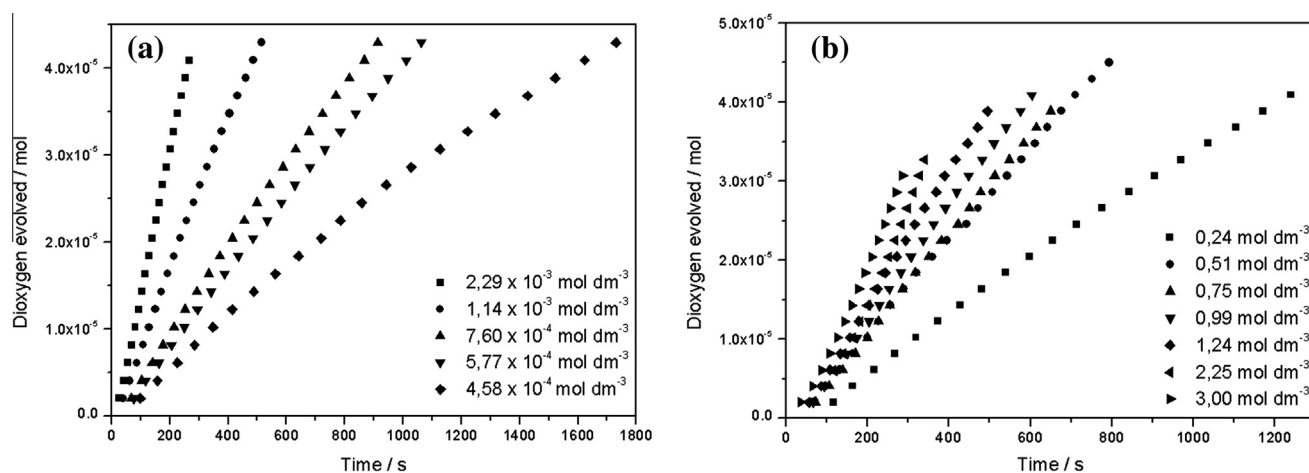


Fig. 6. Evolution of the O_2 from H_2O_2 dismutation catalyzed by $[\text{Fe}_4(\mu\text{-O})(\mu\text{-OH})(\mu\text{-OAc})_4(\text{L})_2](\text{ClO}_4)_3$ in water. (a) $[\text{H}_2\text{O}_2]_0 = 5.00 \times 10^{-1} \text{ mol dm}^{-3}$; $[\text{complex}]_0$ is indicated on the plot. (b) $[\text{complex}]_0 = 1.14 \times 10^{-3} \text{ mol dm}^{-3}$; $[\text{H}_2\text{O}_2]_0$ is indicated on the plot.

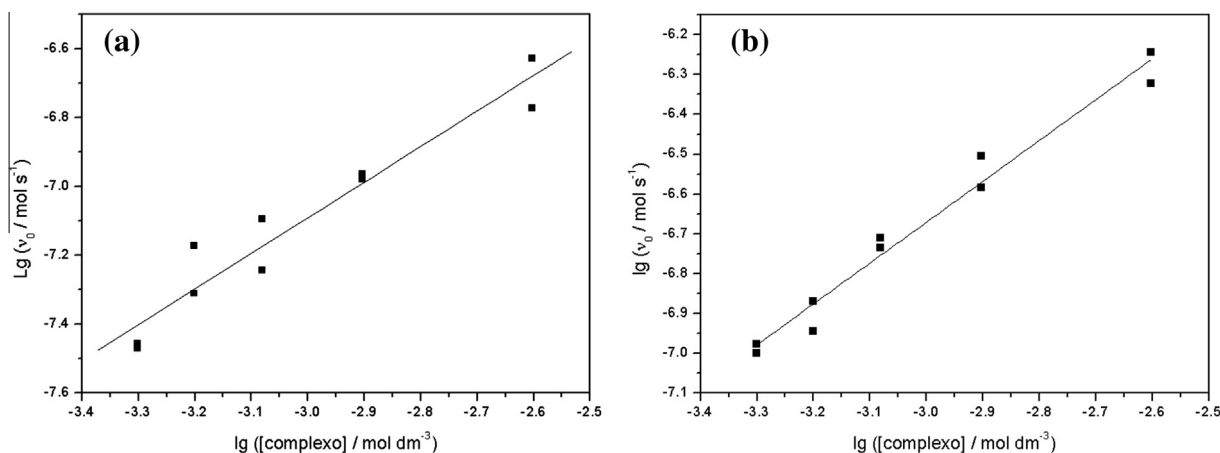


Fig. 7. Lg vs. lg plot of v_0 of O_2 evolution vs. $[\text{complex}]$ ($[\text{Fe}_4(\mu\text{-O})(\mu\text{-OH})(\mu\text{-OAc})_4(\text{L})_2](\text{ClO}_4)_3$) at $[\text{H}_2\text{O}_2]_0 = 5.00 \times 10^{-1} \text{ mol dm}^{-3}$. (a) water and (b) buffer (TRIS 0.25 mol dm^{-3}).

The voltammograms in water (Fig. 5b) show only one redox process, with $E_{\text{pc}}^{(I)} = -0.408 \text{ V}$ versus Ag/AgCl (-0.199 V versus NHE) and $E_{\text{pa}}^{(II)} = 0.113 \text{ V}$ versus Ag/AgCl (0.322 V versus NHE), at

100 mV s^{-1} . The $\Delta E^{(I/II)} = 521 \text{ mV}$ for this process is quite large, being characterized as a *quasi-reversible* process ($\Delta E = 347 \text{ mV}$ for $\text{K}_3[\text{Fe}(\text{CN})_6]$). This process can be attributed to the electron

transfer process $\text{Fe}^{\text{III}}\text{Fe}^{\text{III}}-\text{Fe}^{\text{III}}\text{Fe}^{\text{II}}$. It is important to report that during this analysis an orange precipitate was observed.

3.5. Catalase-like activity

3.5.1. H_2O_2 disproportionation reactions and kinetics experiments

The catalase-like activity promoted by the complex $[\text{Fe}_4(\mu\text{-O})(\mu\text{-OH})(\mu\text{-OAc})_4(\text{L})_2](\text{ClO}_4)_3$ was investigated in order to determine the ability of a synthetic tetranuclear iron complex to disproportionate H_2O_2 . Initially, the disproportionation reactions were investigated in water, the natural environment for catalases. Plots of the amount of dioxygen evolved, measured by volumetry, versus time for each set of experiments, at $[\text{H}_2\text{O}_2]_0$ or $[\text{complex}]_0$ constant, are shown in Fig. 6. The results demonstrate that the complex presents catalase-like activity. After 5 min of reaction, at $[\text{complex}]_0 = 1.14 \times 10^{-3} \text{ mol dm}^{-3}$ and $[\text{H}_2\text{O}_2]_0 = 2.25 \text{ M}$, $2.6 \times 10^{-5} \text{ mol}$ of O_2 were evolved (Fig. 6(b)). Control experiments were conducted under the same conditions with no iron source and only 2.86×10^{-6} dioxygen mol were evolved after 30 min. A control experiment using $\text{Fe}(\text{ClO}_4)_3$ as catalyst in water was also conducted and after 5 min at $[\text{salt}]_0 = 1.08 \times 10^{-3} \text{ mol dm}^{-3}$ and $[\text{H}_2\text{O}_2]_0 = 2.17 \text{ mol dm}^{-3}$, only $5.5 \times 10^{-6} \text{ mol}$ of dioxygen were evolved.

The initial rates method was applied to determine the kinetic parameters and the initial rate values (v_0) were calculated from

the maximum slope of the O_2 versus time curves. The plot of the logarithm of v_0 versus the logarithm of complex concentration (Fig. 7(a)) showed a linear dependence with a slope of 1.04 ± 0.09 , indicating a first-order reaction in relation to the complex in aqueous solutions.

The plot of v_0 vs. $[\text{H}_2\text{O}_2]$ (Fig. 8(a)) could be fit with the Michaelis–Menten equation Eq. (2), revealing a saturation kinetics for the H_2O_2 dismutation by the title complex. Following the recommendations of different authors [72,73], a nonlinear least square fit was applied to calculate the Michaelis–Menten parameters, presented in Table 4.

$$v_0 = k_{\text{cat}}[\text{cat}]_{\text{T}}[\text{S}]_0 / (K_{\text{M}} + [\text{S}]_0), \quad (2)$$

where k_{cat} is the turnover number; K_{M} is the Michaelis constant; $[\text{S}]_0$ is the substrate initial concentration; $[\text{cat}]_{\text{T}}$ is the catalyst concentration.

The K_{M} value equal to 2.88 mol dm^{-3} for the title tetramer in water at pH 7.2 is greater than the values for the natural enzymes from *Thermus thermophilus* ($K_{\text{M}} = 0.083 \text{ mol dm}^{-3}$) [74], *Tricholoma album* ($K_{\text{M}} = 0.015 \text{ mol dm}^{-3}$) [74] and *Lactobacillus plantarum* ($K_{\text{M}} = 0.35 \text{ mol dm}^{-3}$) [73,74], indicating a lower affinity to the substrate. A similar affinity was observed for the tetranuclear manganese model $[\text{Mn}_4(2\text{-OHPicpn})_4](\text{ClO}_4)_4$ ($K_{\text{M}} = 2.6 \pm 0.3 \text{ mol dm}^{-3}$) [21] (entry 7 on Table 4), which presents saturation kinetics retaining the multinuclear structure. The k_{cat} value equal

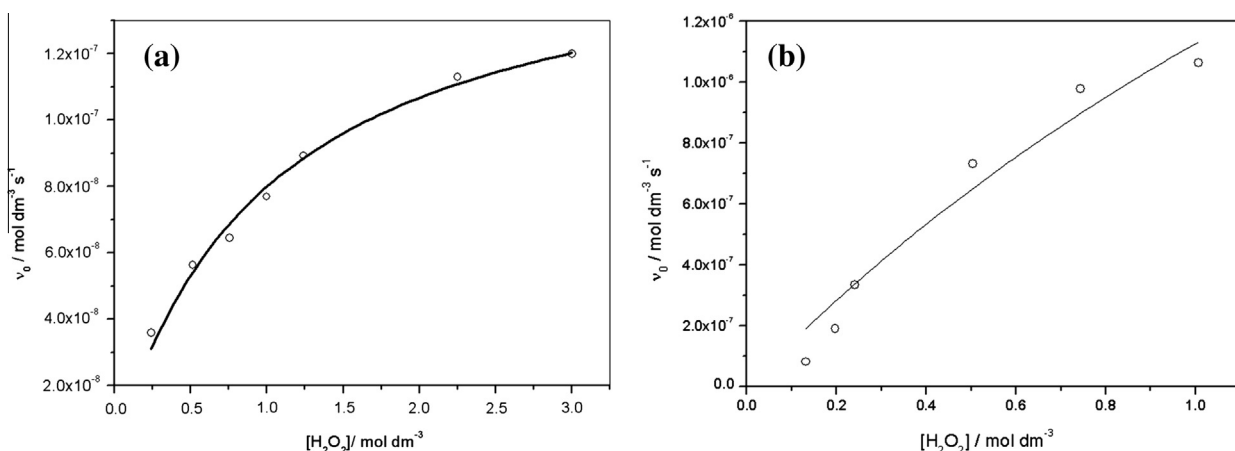


Fig. 8. v_0 of O_2 evolution as a function of $[\text{H}_2\text{O}_2]$. Open circles: experimental data. Continuous line: Nonlinear Least Square fitting using Michaelis–Menten Eq. (2). (a) water, $[\text{complex}]_0 = [\text{cat}]_{\text{T}} = 1.14 \times 10^{-3} \text{ mol dm}^{-3}$; (b) water, pH 7.2 (buffer TRIS 0.25 mol dm^{-3}), $[\text{complex}]_0 = [\text{cat}]_{\text{T}} = 1.25 \times 10^{-3} \text{ mol dm}^{-3}$.

Table 4

Related kinetics values for catalase enzymes and synthetic models.

Entry	Complex/enzyme	K_{M} (M)	k_{CAT} (s^{-1})	$(k_{\text{CAT}}/K_{\text{M}})$ ($\text{s}^{-1} \text{ M}^{-1}$)	Solvent	Refs.
1	$[\text{Fe}_4(\mu\text{-O})(\mu\text{-OH})(\mu\text{-OAc})_4(\text{L})_2](\text{ClO}_4)_3$	1.010	1.41×10^{-4}	1.40×10^{-4}	H_2O	this work
2	$[\text{Fe}_4(\mu\text{-O})(\mu\text{-OH})(\mu\text{-OAc})_4(\text{L})_2](\text{ClO}_4)_3$	2.882	3.50×10^{-3}	1.21×10^{-3}	H_2O , pH 7.2	this work
3	$[\text{Fe}_4(\mu\text{-O})(\mu\text{-OH})(\mu\text{-OAc})_4(\text{L})_2](\text{ClO}_4)_3$	0.7489	5.37×10^{-2}	7.17×10^{-2}	CH_3CN	this work
4	<i>T. thermophilus</i>	0.083 (0.008)	2.6×10^5	3.13×10^6	H_2O	Ref. [74]
5	<i>T. album</i>	0.015	2.6×10^4	1.73×10^6	H_2O	Ref. [74]
6	<i>L. plantarum</i>	0.35	2×10^5	0.57×10^6	H_2O	Ref. [74]
7	$[\text{Mn}_4(2\text{-OHPicpn})_4](\text{ClO}_4)_4$	2.6 (0.3)	–	55 (9)	H_2O	Ref. [21]
8	$[\text{Mn}^{\text{III}}(2\text{-OH}(5\text{-MeOsalpn}))_2]$	0.011 (0.002)	4.2 (0.1)	382 (80)	CH_3CN	Ref. [75]
9	$[\text{L}^{\text{I}}\text{Mn}_2(\mu\text{-Oac})](\text{ClO}_4)_2$	0.035 (0.015)	0.1 (0.005)	2.9	98% $\text{CH}_3\text{OH}/2\% \text{H}_2\text{O}$	Ref. [11]
10	$[\text{L}^{\text{I}}\text{Mn}_2(\mu\text{-Oac})](\text{ClO}_4)_2$	0.0003 (0.00004)	2.1 (0.1)	700	89% $\text{H}_2\text{O}/11\% \text{CH}_3\text{OH}$	Ref. [11]
11	$\text{Na}[\text{Mn}_2(3\text{-Me-5-}\text{SO}_3\text{-salpentO})(\mu\text{-MeO})(\mu\text{-AcO})(\text{H}_2\text{O})_3 \cdot 4\text{H}_2\text{O}]$	0.0066 (0.004)	10.5 (2)	$16(1) \times 10^2$	H_2O , pH 10.6	Ref. [76]
12	$[\text{Mn}^{\text{III}}_2(5\text{-Ome-salpentO})(\mu\text{-AcO})(\mu\text{-MeO})(\text{MeOH})_2]\text{Br}$	0.0071(0.004)	2.0(1)	28	CH_3OH	Ref. [18]
13	$[\text{Mn}^{\text{III}}_2(5\text{-Ome-salpentO})(\mu\text{-AcO})(\mu\text{-MeO})(\text{MeOH})_2]\text{Br}$	0.0044(0.003)	1.62(2)	36	DMF	Ref. [18]
14	$[\text{Mn}^{\text{III}}_2(3\text{-Ome-salpentO})(\mu\text{-AcO})(\mu\text{-MeO})(\text{MeOH})_2]\text{Br}$	0.0013(0.002)	6.2(3)	48	CH_3OH	Ref. [18]
15	$[\text{Mn}^{\text{III}}_2(3\text{-Ome-salpentO})(\mu\text{-AcO})(\mu\text{-MeO})(\text{MeOH})_2]\text{Br}$	0.025(0.002)	7.9(3)	32	DMF	Ref. [18]

HL = 1,3-bis[(2-aminoethyl)amino]-2-propanol; 2-OHPicpn = N,N'-bis-1,3-(picolinimine) propan-2-ol; 2-OHsalpnH2 = 1,3-bis(salicylideneamino)propan-2-ol; L^I = N,N,N',N'-tetrakis(2-methylenebenzamidazolyl)-1,3-diaminopropan-2-ol; salpentOH = 1,5-bis(salicylideneamino)pentan-3-ol.

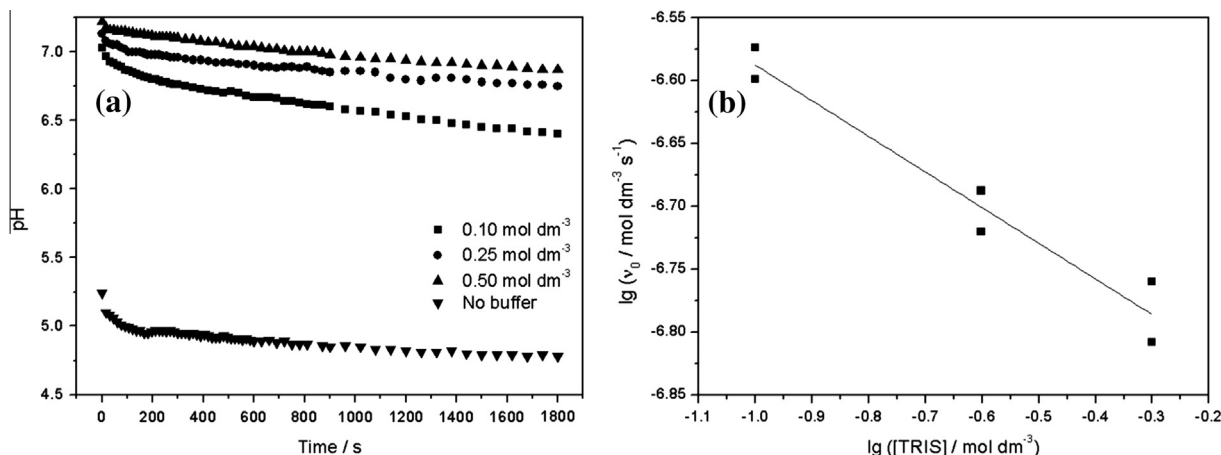


Fig. 9. pH monitoring of the H_2O_2 ($2.5 \times 10^{-1} \text{ mol dm}^{-3}$) disproportionation reaction catalyzed by $[\text{Fe}_4(\mu\text{-O})(\mu\text{-OH})(\mu\text{-OAc})_4(\text{L})_2](\text{ClO}_4)_3$ ($1.25 \times 10^{-3} \text{ M}$). (a) pH variation over time at different TRIS concentration; (b) lg vs. lg plot of v_0 vs. TRIS concentration (angular coefficient = -0.28 ± 0.01 ; $R = 0.94$).

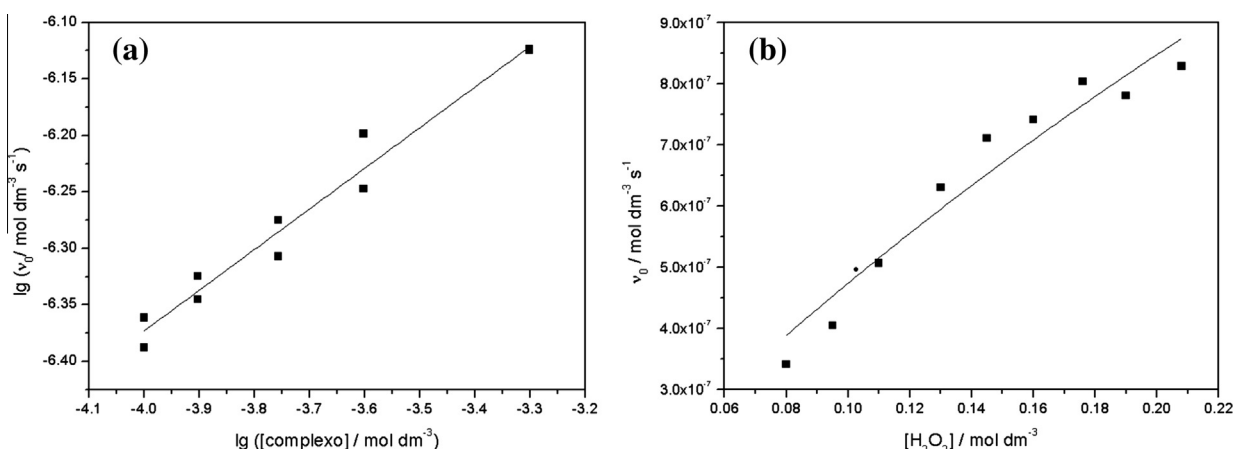


Fig. 10. Kinetics of the H_2O_2 disproportionation in CH_3CN : (a) $\lg(v_0)$ vs. $\lg([\text{complex}]_0)$ at $[\text{H}_2\text{O}_2]_0 = 1.00 \times 10^{-1} \text{ mol dm}^{-3}$ and (b) v_0 vs. $[\text{H}_2\text{O}_2]_0$ at $[\text{complex}]_0 = [\text{cat}]_T = 7.50 \times 10^{-5} \text{ mol dm}^{-3}$.

to $3.50 \times 10^{-3} \text{ s}^{-1}$, however, is quite low when compared to the natural enzymes *T. thermophilus* ($k_{\text{cat}} = 2.6 \times 10^5 \text{ s}^{-1}$) [74], *T. album* ($k_{\text{cat}} = 2.0 \times 10^5 \text{ s}^{-1}$) [74] and *L. plantarum* ($k_{\text{cat}} = 2.6 \times 10^4 \text{ s}^{-1}$) [74]. Despite this iron complex presents lower values of catalytic efficiency than other models [11,18,21,75,76], it must be emphasized that these values were obtained in water and in pH close to the natural, representing an advantage of the title complex with respect to most of the published models, whose studies have been conducted in organic solvent due to the lack of solubility or activity in aqueous solution.

Some authors have observed a pH dependence in the H_2O_2 dismutation [76]. To verify this effect in the studied system, the pH variation over time was monitored during the H_2O_2 disproportionation promoted by $[\text{Fe}_4(\mu\text{-O})(\mu\text{-OH})(\mu\text{-OAc})_4(\text{L})_2](\text{ClO}_4)_3$ and the results are presented in Fig. 9(a). After the addition of H_2O_2 the pH solution immediately decreased from 5.24 to 5.10, and after 200 s the pH had decreased to 4.96, i.e., the pH has changed 0.28 units during the acquirment of the first points used to calculate the initial rates. This pH decrease may be due to the coordination of the peroxide to the complex concomitant with proton release. As the pH decreased, an orange precipitate was formed, which indicates the degradation of the iron complex during the reaction. It is also known that the hydrogen peroxide decomposition is accelerated at high pH. Taking these facts into account, we decided to carry out the experiments in TRIS buffer at pH 7.2, a value close

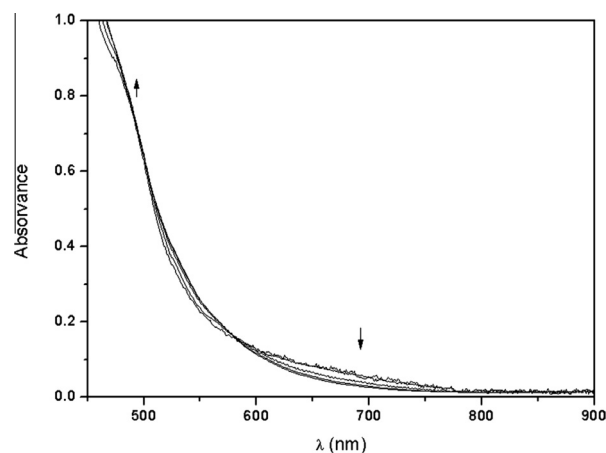


Fig. 11. Spectral changes during the H_2O_2 (0.1 M) disproportionation reaction catalyzed by $[\text{Fe}_4(\mu\text{-O})(\mu\text{-OH})(\mu\text{-OAc})_4(\text{L})_2](\text{ClO}_4)_3$ ($1.5 \times 10^{-3} \text{ M}$) in acetonitrile.

to the biological pH. Monitoring of the reaction pH over time was also carried out in buffer solution at different concentrations, 0.1, 0.25 and 0.50 M, as shown in Fig. 9(a). Although the pH also changed in the buffered solutions, it changed more smoothly as the

buffer concentration increased. In the first 200 s at 0.5 M the variation was of 0.1 unities, at 0.25 M 0.15 unities and at 0.1 M 0.25 unities. In control experiments, in the absence of the complex, the pH solution did not change in presence of H_2O_2 and no significant O_2 volume was evolved, ruling out the hypothesis of oxidative degradation of the TRIS molecules by the hydrogen peroxide.

The coordination of some types of buffers to metal coordination compounds have been described, and in these cases it interferes in the catalytic activity of the complex [77,78]. In order to estimate the TRIS interference in the catalase-like activity of the title

complex, the initial rates were determined in the different buffer concentrations. The logarithm dependence of the initial rate versus buffer concentration is presented in Fig. 9(b) and it was observed that as TRIS concentration increased, the initial rates decreased, so it is likely that the buffer molecules coordinate to the iron center, decreasing its activity. Trying to balance the lost of activity in higher TRIS concentration with the lower efficiency in holding the pH at lower TRIS concentration, the kinetics experiments were carried out in the TRIS concentration of 0.25 M, and the results are shown in Figs. 7(b) and 8(b). The same saturation kinetic behavior

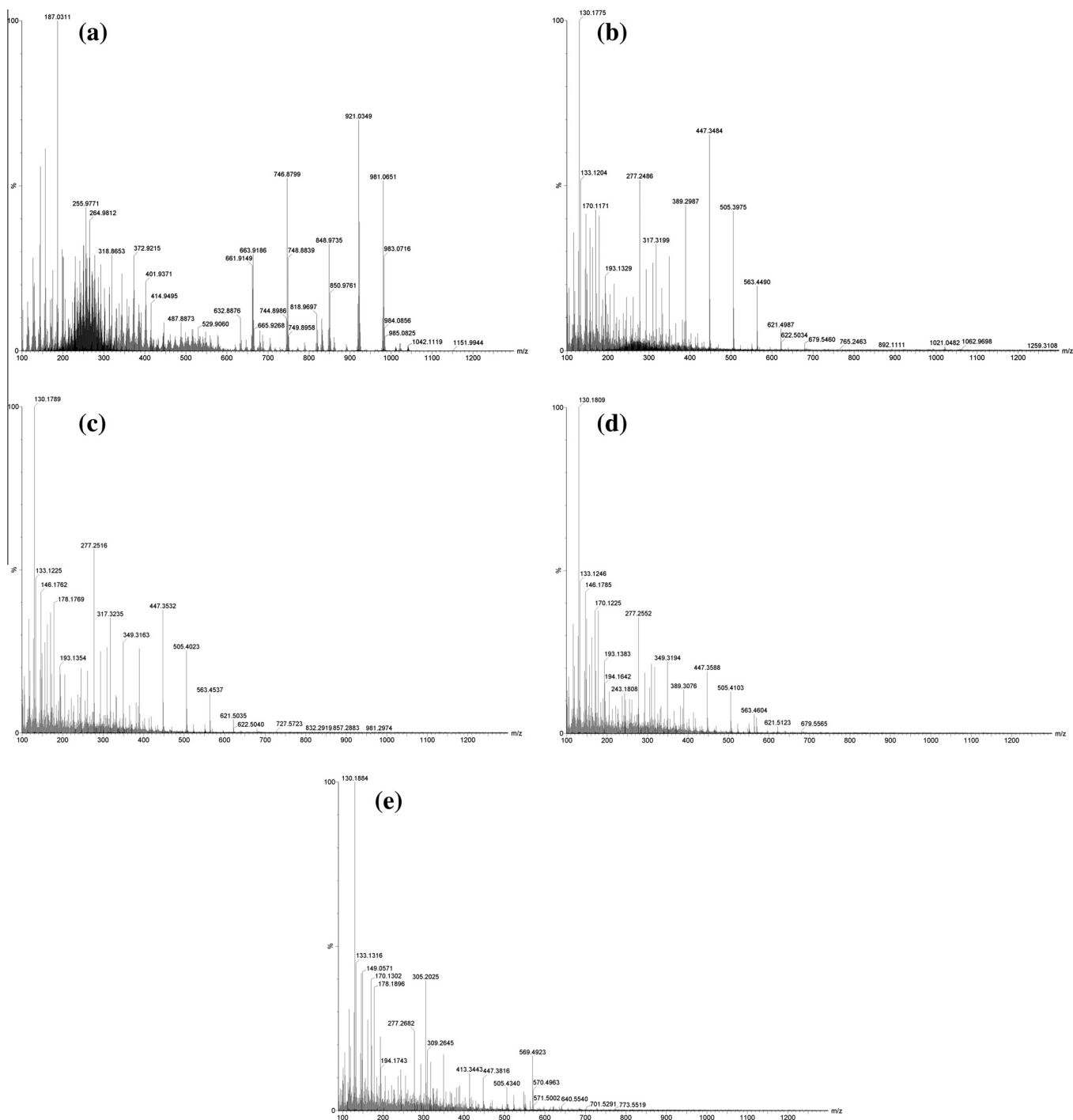


Fig. 12. ESI(+)-MS spectra for the H_2O_2 (0.1 M) disproportionation reaction catalyzed by $[\text{Fe}_4(\mu\text{-O})(\mu\text{-OH})(\mu\text{-OAc})_4(\text{L})_2](\text{ClO}_4)_3$ (1.0×10^{-5} M) in acetonitrile. (a) before the H_2O_2 addition; (b) after 0.2 min; (c) 3 min; (d) 9 min and (e) 20 min of the H_2O_2 addition.

was obtained in buffer, with first-order (1.03 ± 0.06) in relation to the complex and a k_{obs} of $3.50 \times 10^{-3} \text{ s}^{-1}$, 25-fold higher than in water.

The catalytic efficiency of the title complex was also studied in acetonitrile (Fig. 10) in order to compare with published data, since most of the available kinetic experiments for synthetic models were carried out in organic solvent. k_{cat} (5.37×10^{-2}) in CH_3CN was 381-fold higher than in water and 15-fold higher than in buffer. The same trend is reported for other complexes [76], some authors have shown that the catalase-like activity is accelerated at higher pH values as well as in aprotic solvents as acetonitrile. Probably, a high concentration of protons is capable of generating inactive or less active species. The difference between the catalytic efficiency in aqueous solution and in acetonitrile may also be related to the different electron transfer rates in both solvents, as evidenced by the cyclic voltammetry analyses. Furthermore, when the experiments were performed in water a precipitate was formed, indicating a faster decomposition of the initial complex.

3.5.2. Progress of H_2O_2 disproportionation reactions followed by UV-Vis, ESI-MS/Q-TOF and EPR

The catalase-like activity of the title complex in water, in buffer and in acetonitrile was monitored by electronic spectroscopy. The aqueous and buffered solutions presented similar spectra, as shown in Fig. 3(a). During the reaction, no significant change was observed besides the increase of the spectral line in the region of 500–900 nm (Fig. S4), which can be originated from light dispersion caused by suspended particles. The spectral line increased faster in water than in buffer and it is associated to the orange precipitate observed during the experiments. These results also indicate that the generation of the precipitate is pH-dependent.

Different from the aqueous solutions, in acetonitrile an isosbestic point was observed around 600 nm, with the decay of the band at 675 nm and the increasing in the intensity of the band at 550 nm (Fig. 11). As the band at 675 nm was attributed to the Fe–O–Fe core, its disappearance indicates that the new species formed does not possess an oxo bridge.

Since ESI is a gentle ionization technique and causes little or no fragmentation of the sample, it has been used extensively to study reaction mechanisms involving organic or inorganic species [79]. The ESI(+)-MS spectrum of the complex in acetonitrile (Fig. 12) showed the presence of a few low molecular weight mononuclear species with the compositions $[\text{Fe}^{\text{II}}(\mu\text{-OH})(\mu\text{-O})]^+$ (m/z 145), $[\text{Fe}^{\text{II}}(\mu\text{-O})(\mu\text{-OAc})]^+$ (m/z 187), $[\text{Fe}^{\text{III}}(\mu\text{-OAc})_3\text{Na}]^+$ (m/z 256) and $[\text{Fe}^{\text{II}}_2(\mu\text{-O})_2(\mu\text{-OAc})_2(\text{H}^+)_3]^+$ (m/z 265), and some tetranuclear species with the compositions $[\text{Fe}^{\text{II}}_4(\mu\text{-O})(\mu\text{-OAc})(\text{L-H}^+)(\text{L})(\text{ClO}_4)]^+$ (m/z 747), $[\text{Fe}^{\text{II}}_4(\mu\text{-OAc})_3(\text{L-H}^+)(\text{L})(\text{ClO}_4)]^+$ (m/z 849), $[\text{Fe}^{\text{II}}_4(\mu\text{-O})_2(\mu\text{-OAc})_2(\text{L-H}^+)(\text{L})(\text{ClO}_4)_2]^+$ (m/z 920) and $[\text{Fe}^{\text{III}}_4(\mu\text{-O})_2(\mu\text{-OAc})_3(\text{L})(\text{ClO}_4)_2]^+$ (m/z 981). This indicates that the solid-state structure is not well preserved in acetonitrile, but some of the species formed in solution still maintain the tetranuclear core.

In order to get some information about the mechanism, the reaction of the complex with H_2O_2 was monitored by ESI(+)-MS in acetonitrile at room temperature. H_2O_2 was added to the complex solution, which was directly infused into the ESI source of a Q-TOF mass spectrometer. The spectra are presented in Fig. 12 and they were recorded before the addition of the substrate and after 0.2, 3, 9 and 20 min the reaction has started. The addition of H_2O_2 immediately caused a major shift in the spectrum, only peaks in the range of 100–650 m/z were observed and any of these peaks refers to a tetranuclear core. Peaks in the range of 100–250 m/z may refer to low molecular weight complexes caused by the cleavage of the complex in solution. The series of ions above 400 m/z differing by m/z 58 repeating units is not related to an iron-containing species since the characteristic first peak from the iron isotope pattern is absent. They can be attributed to the

cluster $[(\text{L})_2(\text{Na}^+)_3\text{N}_2]^+$, m/z 447.2879, with units of propylene oxide, probably from the plastic bottle of the H_2O_2 . The species between 250–400 m/z can be assigned to iron mononuclear complexes with compositions $[\text{Fe}^{\text{II}}(\text{L})(\text{H}_2\text{O})\text{N}_2]^+$, $[\text{Fe}^{\text{III}}(\text{L})(\mu\text{-OH})(\text{CH}_3\text{CN})\text{N}_2]^+$, $[\text{Fe}^{\text{II}}(\text{L})(\text{H}_2\text{O})_4\text{N}_2]^+$, $[\text{Fe}^{\text{II}}(\text{L})(\text{H}_2\text{O})_5\text{N}_2]^+$ and $[\text{Fe}^{\text{III}}(\text{L})(\mu\text{-OH})(\text{CH}_3\text{CN})(\text{H}_2\text{O})_4\text{N}_2]^+$ of m/z 277, 317, 331, 349 and 389, respectively. The peak of m/z 305 increases with time and does not refer to an iron species, it can be attributed to the cluster $[(\text{L})(\text{Na}^+)_2(\text{N}_2)_3]^+$ and indicates the complex degradation over time. A control test where pure water was added to the solution instead of hydrogen peroxide showed no changes from the original complex spectrum. We conclude that the active species in acetonitrile is a mononuclear species.

EPR spectra of the complex in presence of H_2O_2 were also collected in CH_3CN at 77 K, from 0 to 20 min of reaction (Fig. S7). All the measurements furnished EPR silent spectra. This is in agreement with the ESI(+)-MS experiments, once the majority of the species formed after reaction with peroxide are Fe(II) and EPR silent. Similar results were found for the binuclear complex $[\text{Fe}_2\text{-O}(\text{bipy})_4(\text{OH})_2][\text{ClO}_4]_4$, where the final products of the reaction were mononuclear iron(II) and iron(III) species [25]. We believe that in our case the concentration of the iron(III) species observed on the ESI(+)-MS spectra are too low to give an EPR signal.

3.6. Cyclohexane oxidation

Some authors [25,27] have described the competition between hydrogen peroxide dismutation and oxidation chemistry, when a substrate is present, using (μ -oxo)diiron(III) complexes. In order to verify if the title tetranuclear complex is promiscuous or selective for either catalase- or monooxygenase-like activity, we carried out the cyclohexane oxidation with $[\text{Fe}_4(\mu\text{-O})(\mu\text{-OH})(\mu\text{-OAc})_4(\text{L})_2][\text{ClO}_4]_3$ and H_2O_2 , in CH_3CN . The oxidized products (measured after 24 h), cyclohexanol and cyclohexanone, were formed in small yields (yield cyclohexanol/cyclohexanone: 0.8/0.7% (25 °C) and 2.9/2.6% (50 °C)). Cyclohexyl hydroperoxide was also formed (10.2 at 25 °C and 28.1 at 50 °C), being the major product in both temperatures. Control experiments were conducted under the same conditions with no iron source and no oxidation of cyclohexane was observed in both temperatures. Control experiments using $\text{Fe}(\text{ClO}_4)_3$ as catalyst were also conducted and the yields of cyclohexanol (1.8% at 25 °C; 1.4 at 50 °C) and cyclohexanone (2.2% at 25 °C; 1.1 at 50 °C) were comparable to the values obtained with the tetramer in both temperatures. Cyclohexyl hydroperoxide (2.9% at 25 °C; 42.4 at 50 °C) was also the major product. These results reinforce the low monooxygenase activity of the tetranuclear complex, which oxidation of cyclohexane are in the level of iron(III) salts and no influence from the ligand was observed. Cyclohexane oxidation using iron(III) salts has been reported previously, where high yields were obtained, with cyclohexyl hydroperoxide as the major product as well [80]. Therefore, $[\text{Fe}_4(\mu\text{-O})(\mu\text{-OH})(\mu\text{-OAc})_4(\text{L})_2][\text{ClO}_4]_3$ seems to prefer the pathway that leads to the active species involved in the H_2O_2 decomposition than those toward oxidation chemistry [25,27].

4. Conclusions

In summary, the complex $[\text{Fe}_4(\mu\text{-O})(\mu\text{-OH})(\mu\text{-OAc})_4(\text{L})_2][\text{ClO}_4]_3$ was synthesized through the reaction between the known ligand (1,3-bis[(2-aminoethyl)amino]-2-propanol) and the salts $\text{Fe}(\text{ClO}_4)_3 \cdot x\text{H}_2\text{O}$ and $\text{NaOAc} \cdot 3\text{H}_2\text{O}$, and possesses a (μ -oxo)(μ -hydroxo)bis(μ -alkoxo)tetra(μ -carboxylato)tetrairon core. The complex shows catalase-like activity in water, in TRIS buffer and in CH_3CN . The kinetic experiments results revealed a Michaelis–Menten behavior in relation to the H_2O_2 and a first-order kinetic in

relation to the complex. It was shown a strong pH dependence in the catalytic activity and stability of the complex, low pH disfavors both. Complex decomposition was supported by UV–Vis and ESI-MS experiments, being more critical in presence of high concentration of proton. The catalytic activity was higher in CH₃CN than in aqueous solution, following the order: $k_{\text{obs}}(\text{CH}_3\text{CN}) > k_{\text{obs}}(\text{buffers}) > k_{\text{obs}}(\text{H}_2\text{O})$. Mononuclear species are the most probable catalytic species in acetonitrile.

Acknowledgments

We acknowledge CNPq and FAPERJ for financial support, Laboratório de Difração de Raios X (LDRX) from Universidade Federal Fluminense (UFF) for the diffractometer facility, Laboratório Multiusuário de Espectrometria de Massas (LABEM) of Universidade Federal do Rio de Janeiro (UFRJ) for the ESI-MS spectra and to Laboratório Regional Sul de EPR from Universidade Federal do Paraná (UFPR) for the EPR experiments.

Appendix A. Supplementary material

CCDC 794367 contains the supplementary crystallographic data for this paper. These data can be obtained free of charge from The Cambridge Crystallographic Data Centre via www.ccdc.cam.ac.uk/data_request/cif. Supplementary data associated with this article can be found, in the online version, at <http://dx.doi.org/10.1016/j.ica.2013.07.034>.

References

- [1] S. Choua, P. Pacheco, C. Coquelet, E. Bienvenüe, *J. Inorg. Biochem.* 65 (1997) 79.
- [2] M. Zámocký, F. Koller, *Prog. Biophys. Mol. Biol.* 72 (1999) 19.
- [3] C. Jakopitsch, M. Auer, G. Regelsberger, W. Jantschko, P.G. Furtmüller, F. Rölker, C. Obinger, *Biochemistry* 42 (2003) 5292.
- [4] P. Chelikani, X. Carpena, R. Perez-Luque, L.J. Donald, H.W. Duckworth, J. Switala, I. Fita, P.C. Loewen, *Biochemistry* 44 (2005) 5597.
- [5] I. Fita, A.M. Silva, M.R.N. Murthy, M.G. Rossmann, *Acta Crystallogr., Sect. B* 42 (1986) 497.
- [6] I. Fita, M.G. Rossmann, *J. Mol. Biol.* 185 (1985) 21.
- [7] B.K. Vainshtein, W.R. Melik-Adamyán, V.V. Barynin, A.A. Vagin, A.I. Grebenko, V.V. Borisov, K.S. Bartels, I. Fita, M.G. Rossmann, *J. Mol. Biol.* 188 (1986) 49.
- [8] S.V. Antonyuk, V.R. Melik-Adamyán, A.N. Popov, V.S. Lamzin, P.D. Hempstead, P.M. Harrison, P.J. Artymyuk, V.V. Barynin, *Crystallogr. Rep.* 45 (2000) 105.
- [9] V.V. Barynin, M.M. Whittaker, S.V. Antonyuk, V.S. Lamzin, P.M. Harrison, P.J. Artymyuk, *J.W. Whittaker, Structure* 9 (2001) 725.
- [10] J. Gao, A.E. Martell, J.H. Reibenspies, *Inorg. Chim. Acta* 346 (2003) 32.
- [11] A.E.M. Boelrijk, G.C. Dismukes, *Inorg. Chem.* 39 (2000) 3020.
- [12] J. Paschke, M. Kirsch, H.-G. Korth, H. Groot, R. Sustmann, *J. Am. Chem. Soc.* 123 (2001) 11099.
- [13] J. Kaizer, T. Csay, P. Kóvári, G. Speier, L. Párkányi, *J. Mol. Catal. A: Chem.* 280 (2008) 203.
- [14] M. McCann, M.T. Casey, M. Devereux, M. Curran, C. Cardin, A. Todd, *Polyhedron* 15 (1996) 2117.
- [15] S. McCann, M. McCann, M.T. Casey, M. Jackman, M. Devereux, V. McKee, *Inorg. Chim. Acta* 279 (1998) 24.
- [16] A. Gelasco, V.L. Pecoraro, *J. Am. Chem. Soc.* 115 (1993) 7928.
- [17] E.J. Larson, V.L. Pecoraro, *J. Am. Chem. Soc.* 113 (1991) 7809.
- [18] C. Palopoli, M. González-Sierra, G. Robles, F. Dahan, J.-P. Tuchagues, S. Signorella, *J. Chem. Soc., Dalton Trans.* (2002) 3813.
- [19] D. Moreno, C. Palopoli, V. Daier, S. Shova, L. Vendier, M. González Sierra, J.-P. Tuchagues, S. Signorella, *Dalton Trans.* (2006) 5156.
- [20] H. Biava, C. Palopoli, S. Shova, M. Gaudio, V. Daier, M. González-Sierra, J.-P. Tuchagues, S. Signorella, *J. Inorg. Biochem.* 100 (2006) 1660.
- [21] A. Gelasco, A. Askenas, V.L. Pecoraro, *Inorg. Chem.* 35 (1996) 1419.
- [22] T.H. Bennur, D. Srinivas, S. Sivasanker, V.G. Puranik, *J. Mol. Catal. A: Chem.* 219 (2004) 209.
- [23] C.E. Dube, D.W. Wright, W.H. Armstrong, *Angew. Chem., Int. Ed.* 39 (2000) 2169.
- [24] B. Mauere, J. Crane, J. Schuler, K. Wiegardt, B. Nuber, *Angew. Chem., Int. Ed.* 32 (1993) 289.
- [25] S. Ménage, J.M. Vincent, C. Lambeaux, M. Fontecave, *J. Chem. Soc., Dalton Trans.* (1994) 2081.
- [26] S. Ito, T. Okuno, H. Matsushima, T. Tokii, Y. Nishida, *J. Chem. Soc., Dalton Trans.* (1996) 4479.
- [27] T. Okuno, S. Ito, S. Ohba, Y. Nishida, *J. Chem. Soc., Dalton Trans.* (1997) 3547.
- [28] S. Nishino, H. Hosomi, S. Ohba, H. Matsushima, T. Tokii, Y. Nishida, *J. Chem. Soc., Dalton Trans.* (1999) 1509.
- [29] N.M.F. Carvalho, A. Horn Jr., R.B. Faria, A.J. Bortoluzzi, V. Drago, O.A.C. Antunes, *Inorg. Chim. Acta* 359 (2006) 4250.
- [30] A. Horn Jr., G.L. Parrilha, K.V. Melo, C. Fernandes, M. Horner, L.C. Visentin, J.A.S. Santos, M.S. Santos, E.C.A. Eleutherio, M.D. Pereira, *Inorg. Chem.* 49 (2010) 1274.
- [31] I.-P. Lorenz, W. Pohl, H. Nöth, *Angew. Chem., Int. Ed.* 36 (1997) 55.
- [32] K.-H. Lii, Y.-F. Huang, *Chem. Commun.* (1997) 839.
- [33] H. Li, Z.J. Zhong, W. Chen, X.Z. You, *J. Chem. Soc., Dalton Trans.* (1997) 463.
- [34] B.P. Murch, F.C. Bradley, P.D. Boyle, V. Papaefthymiou, L. Que Jr., *J. Am. Chem. Soc.* 109 (1987) 7993.
- [35] S. Drüeke, K. Wiegardt, B. Nuber, J. Weiss, E.L. Bominaar, A. Sawaryn, H. Winkler, A.X. Trautwein, *Inorg. Chem.* 28 (1989) 4477.
- [36] J.L. Sessler, J.W. Sibert, A.K. Burrell, V. Lynch, J.T. Markert, C.L. Wooten, *Inorg. Chem.* 32 (1993) 4277.
- [37] H. Toftlund, K.S. Murray, P.R. Zwack, L.F. Taylor, O.P. Anderson, *J. Chem. Soc., Chem. Commun.* (1986) 191.
- [38] J.L. Sessler, J.W. Sibert, V. Lynch, *Inorg. Chem.* 29 (1990) 4143.
- [39] J.L. Sessler, J.D. Hugdahl, V. Lynch, B. Davis, *Inorg. Chem.* 30 (1991) 334.
- [40] J.L. Sessler, J.W. Sibert, V. Lynch, J.T. Markert, C.T. Wooten, *Inorg. Chem.* 32 (1993) 621.
- [41] N. Arulsamy, J. Glerup, D.J. Hodgson, *Inorg. Chem.* 33 (1994) 3043.
- [42] Q. Chen, J.B. Lynch, P. Gomez-Romero, A. Ben-Hussein, G.B. Jameson, C.J. O'Connor, L. Que Jr., *Inorg. Chem.* 27 (1988) 2673.
- [43] D.L. Jameson, C.-L. Xie, D.N. Hendrickson, J.A. Potenza, H.J. Schugar, *J. Am. Chem. Soc.* 109 (1987) 740.
- [44] A.K. Boudalis, N. Lalioti, G.A. Spyroulias, C.P. Raptopoulou, A. Terzis, A. Bousseksou, V. Tangoulis, J.-P. Tuchagues, S.P. Perlepes, *Inorg. Chem.* 41 (2002) 6474.
- [45] Y.-S. Xie, X.-T. Liu, M. Zhang, K.-J. Wei, Q.-L. Liu, *Polyhedron* 24 (2005) 165.
- [46] R.R. Gagne, C.A. Koval, G.C. Lisensky, *Inorg. Chem.* 19 (1980) 2854.
- [47] P.T. Kissinger, *Laboratory Techniques in Electroanalytical Chemistry*, second ed., Marcel Dekker, Inc., New York, 1996.
- [48] Nonius, COLLECT. Nonius BV, Delft, The Netherlands, 1998.
- [49] A.J.M. Duisenberg, R.W.W. Hooft, A.M.M. Schreurs, J. Kroon, *J. Appl. Crystallogr.* 33 (2000) 893.
- [50] A.J.M. Duisenberg, *J. Appl. Crystallogr.* 25 (1992) 92.
- [51] A.J.M. Duisenberg, L.M.J. Kroon-Batenburg, A.M.M. Schreurs, *J. Appl. Crystallogr.* 36 (2003) 220.
- [52] G.M. Sheldrick, SADABS, Program for Empirical Absorption Correction of Area Detector Data, University of Göttingen, Germany, 1996.
- [53] G.M. Sheldrick, SHELXS97, Program for Crystal Structure solution, University of Göttingen, Germany, 1997.
- [54] G.M. Sheldrick, SHELXL97, Program for crystal structure refinement, University of Göttingen, Germany, 1997.
- [55] A.L. Spek, *J. Appl. Crystallogr.* 36 (2003) 7.
- [56] G.B. Shul'pin, Y.N. Kozlov, L.S. Shul'pina, P.V. Petrovskiy, *Appl. Organomet. Chem.* 24 (2010) 464.
- [57] A. Horn, A. Neves, A.J. Bortoluzzi, V. Drago, W.A. Ortiz, *Inorg. Chem. Commun.* 4 (2001) 173.
- [58] J.H. Satcher Jr., M.M. Olmstead, M.W. Droegge, S.R. Parkin, B.C. Noll, L. May, A.L. Balch, *Inorg. Chem.* 37 (1998) 6751.
- [59] C. Fernandes, A. Neves, I. Vencato, A.J. Bortoluzzi, V. Drago, T. Weyhermueller, E. Rentschler, *Chem. Lett.* (2000) 540.
- [60] J.H. Satcher Jr., M.W. Droegge, M.M. Olmstead, A.L. Balch, *Inorg. Chem.* 40 (2001) 1454.
- [61] M. Costas, C.W. Cady, S.V. Kryatov, M. Ray, M.J. Ryan, E.V. Rybak-Akimova, L. Que Jr., *Inorg. Chem.* 42 (2003) 7519.
- [62] T. Tanase, C. Inoue, E. Ota, S. Yano, M. Takahashi, M. Takeda, *Inorg. Chim. Acta* 297 (2000) 18.
- [63] A.K. Boudalis, V. Tangoulis, C.P. Raptopoulou, A. Terzis, J.-P. Tuchagues, S.P. Perlepes, *Inorg. Chim. Acta* 357 (2004) 1345.
- [64] T. Tanase, T. Inagaki, Y. Yamada, M. Kato, E. Ota, M. Yamazaki, M. Sato, W. Mori, K. Yamaguchi, M. Mikuriya, M. Takahashi, M. Takeda, I. Kinoshita, S. Yano, *J. Chem. Soc., Dalton Trans.* (1998) 713.
- [65] G.B. Deacon, R.J. Phillips, *Coord. Chem. Rev.* 33 (1980) 227.
- [66] R.E. Norman, R.C. Holz, S. Ménage, C.J. O'Connor, J.H. Zhang, L. Que Jr., *Inorg. Chem.* 29 (1990) 4629.
- [67] R.C. Holz, T.E. Elgren, L.L. Pearce, J.H. Zhang, C.J. O'Connor, L. Que Jr., *Inorg. Chem.* 32 (1993) 5844.
- [68] H. Zheng, Y. Zang, Y. Dong, V.G. Young Jr., L. Que Jr., *J. Am. Chem. Soc.* 121 (1999) 2226.
- [69] D. Li, Z. Liao, Y. Wei, F. Du, M. Wang, W. Chen, W. Li, X. Mao, *Dalton Trans.* (2003) 2164.
- [70] G.A. Mabbott, *J. Chem. Educ.* 60 (1983) 697.
- [71] J. Mukherjee, V. Balamurugan, R. Gupta, R. Mukherjee, *Dalton Trans.* (2003) 3686.

- [72] J.H. Espenson, *Chemical Kinetics and Reaction Mechanisms*, second ed., McGraw-Hill, New York, 2002. p. 91.
- [73] S. Signorella, A. Rompel, K. Büldt-Karentzopoulos, B. Krebs, V.L. Pecoraro, J.-P. Tuchagues, *Inorg. Chem.* 46 (2007) 10864.
- [74] M. Shank, V. Barynin, G.C. Dismukes, *Biochemistry* 33 (1994) 15433.
- [75] A. Gelasco, S. Benzie, V.L. Pecoraro, *Inorg. Chem.* 37 (1998) 3301.
- [76] C. Palopoli, N. Bruzzo, C. Hureau, S. Ladeira, D. Murgida, S. Signorella, *Inorg. Chem.* 50 (2011) 8973.
- [77] B.E. Fischer, U.K. Häring, R. Tribolet, H. Sigel, *Eur. J. Biochem.* 94 (1979) 523.
- [78] H. Sigel, K. Wyss, B.E. Fischer, B. Prijs, *Inorg. Chem.* 18 (1979) 1354.
- [79] J.A. Lessa, A. Horn Jr., E.S. Bull, M.R. Rocha, M. Benassi, R.R. Catharino, M.N. Eberlin, A. Casselato, C.J. Noble, G.R. Hanson, G. Schenk, G.C. Silva, O.A.C. Antunes, C. Fernandes, *Inorg. Chem.* 48 (2009) 4569.
- [80] B. Retcher, J.S. Costa, J. Tang, R. Hage, P. Gamez, J. Reedijk, *J. Mol. Catal. A: Chem.* 286 (2008) 1.